FORMATION OF HIGH MOLECULAR WEIGHT AROMATICS IN FUEL-RICH FLAMES

Jack B. Howard

Fuels Research Laboratory, Department of Chemical Engineering
Massachusetts Institute of Technology
Cambridge, Massachusetts 02139

GENERAL OBSERVATIONS

Gas composition measurements as a function of distance or time through the reaction zone of fuel-rich premixed flames reveals the occurrence of high molecular weight aromatics formed by growth reactions that accompany the destruction of the fuel. The lumped concentration profile of all species heavier than molecular weight M exhibits a sharp peak (Fig. 1) indicative of net production of heavy material giving way to net consumption during passage through the reaction zone of the flame (from left to right in the figure). The data in Fig. 1 were obtained by probing along the centerline of a low-pressure, one-dimensional or plug-flow premixed acetylene-oxygen flame using a molecular-beam forming sampling instrument with on-line mass spectrometry. The heavy aromatics at flame temperatures, here about 1800 K, include both ions and neutrals. The heavy ions profile in Fig. 1, obtained (1) with a Faraday cage and electrical deflection of the molecular beam in the sampling instrument (2), includes ions larger than about 300 amu. The profile for M > 1000 amu species, obtained (3) with an on-line quadrupole mass spectrometer in the sampling instrument (Fig. 2), includes both ions and neutrals. The reactions involved are rapid, 3 mm of distance in Fig. 2 corresponding to a time interval of about 1 ms. When the fuel equivalence ratio [ϕ = (fuel/oxygen)/(fuel/oxygen) stoichiometric] is above the critical value for soot formation, it is at the location of the peak concentration of the heavy aromatic compounds that the soot particles begin to form (4). When soot formation is impending, an increase of fuel/oxygen ratio by only a few percent gives a 100-fold increase in the peak concentration of the heavy aromatics.

RESOLUTION OF MOLECULAR WEIGHT GROWTH

In order to gain more understanding of the evolution of heavy hydrocarbons, mass spectrometer intensity profiles such as that for $I_{M>1000}$ in Fig. 1 but with the cutoff mass M varied in 50 amu steps from 200 amu to 750 amu were measured in a near-sooting low-pressure (2.67 kPa) C_6H_6/O_2 flame (4,5). If $I_{M>1000}$ is the signal intensity of all species of molecular weight M greater than the cutoff value m, then a probability distribution function (p.d.f.) $f_{200}(m)$ can be defined as

$$f_{200}(m) = -d[I_{M>m}/I_{M>200}]/dm$$

where $f_{200}(m)$ represents the number fraction of all species greater than 200 amu lying in the range m to m + dm.

The p.d.f.'s for five distances from the burner (5) are shown in Fig. 3. The p.d.f. at 7.95 mm is heavily weighted toward the mass range 200-300 amu. As the distance from the burner increases, the p.d.f. increases at the higher masses and decreases at the lower masses. At distances above 10.0 mm, the signal between 200 and 300 amu is a small to negligible fraction of the total, and the distributions are relatively uniform in the range 300-600 amu. At 10.9 and 12.1 mm, the distributions turn upward at the far right indicative of a faster growth of the higher-mass species, but it is not known if this apparent behavior is real or an artifact of the data at this high-mass extreme of the mass range studied.

These observations show that although the number density of high molecular weight species decreases with distance from the burner beyond the location of the

maximum concentration (e.g., Fig. 1), the mean molecular weight continually increases. In order to determine how the total mass of heavy species changes as the number decreases, the p.d.f. has been multiplied by m to convert to a mass basis and by

$$I_{M>200}/(I_{M>200})_{z=7.95mm}$$

to normalize the mass with the constant number of moles of heavy material existing at an arbitrarily fixed distance (z = 7.95 mm) from the burner. The resulting function,

$$mf_{200}(m)I_{M>200}/(I_{M>200})_{z=7.95mm}$$

is shown in Fig. 4 for different molecular weights as a function of distance from the burner (5). A point on one of the curves represents the mass of species of the indicated molecular weight existing at the indicated distance from the burner, expressed as a ratio to the total number of moles of M>200 amu material existing at 7.95 mm.

It can be seen in Fig. 4 that the mass of material at a given molecular weight exhibits a peak at a height above burner which increases with increasing mass number. The shapes of the curves and the location of the peaks are the same as would be seen if number of moles instead of mass were plotted, since the number curves could be produced by vertical displacement of each mass curve in accordance with division by the constant molecular weight indicated thereon. In comparison with mole fraction profiles for individually identified species of m less than or equal to 200 amu, shown later, the curves in Fig. 4 constitute a continuation of the progression seen for the individual hydrocarbon species, namely molar concentration profiles peaking as m increases. Figure 4 shows that the peak concentrations also decrease as m increases. The mean molecular weight and overall mass and number concentrations of the high-mass material (5) are shown in Fig. 5.

INTERPRETED GROWTH BEHAVIOR

The above information shows that the rapid decrease in number concentration of heavy species that occurs immediately downstream of the peak concentration (Fig. 1) is not only accompanied by increasing mean molecular weight but also a net consumption or loss of material. Whether this consumption is due to oxidation, pyrolysis, or a combination of these has been addressed (5) by calculation of fluxes of O_2 and hydrocarbon species at the beginning and end of the zone of the heavy species consumption, both for the above near-sooting flame data and for similar data from a sooting C_6H_6/O_2 flame operated under otherwise identical conditions. The fraction of the initial oxygen remaining as O_2 at the beginning of the zone of rapid consumption of M>700 amu material is 37.2% and 18.3% for the near-sooting and sooting flames, respectively, and the O_2 remaining at the end of the zone of rapid consumption of M>700 amu material is about 1% of the initial value in both flames. Therefore the amount of oxidation occurring within this zone is indeed substantial, thus allowing the possibility that oxidation plays a role in the destruction of the high-mass material or its pyrolytic decomposition products. It is also found that the amount of M>700 amu material increases by a factor of 100 in going from the nearly sooting to the sooting case, even though the benzene fed is only increased by about 10%. In addition, the benzene fuel is almost gone when the M>700 material reaches its maximum concentration, indicating that the amount of these heavy species continues to increase as long as benzene is available. This behavior may mean that the concentration of oxidizing radicals that consume heavy species is suppressed by reaction with benzene, and also that benzene serves as a source of growth species for the heavy material. When the heavy species are undergoing rapid consumption, an even larger quantity of the prevalent intermediate, acetylene, is being consumed. Consequently, with regard to the molecular weight growth that accompanies the destruction of heavy compounds, acetylene and related species such as diacetylene (C_4H_2) and vinylacetylene (C_4H_4) may be important reactants.

IDENTIFIED SPECIES

Species and reactions involved in the early stages of the formation of high molecular weight compounds were studied (3,4) in the near-sooting C_6H_6/O_2 flame discussed above using the instrument shown in Fig. 2. Measured mole fraction profiles from which species fluxes and net reaction rates were computed are presented in Figs. 6-10. It will be noted in these figures that numerous intermediates are involved whose formation and subsequent destruction exhibit a general trend to larger molecular weights and smaller peak concentrations. It is this progression or sequential growth that is mentioned above as continuing on to the high molecular weight species. This behavior in both the near-sooting C_6H_6/O_2 flame and the sooting C_2H_2/O_2 flame discussed above is illustrated in Fig. 11 where the mole fractions of selected compounds are plotted with the intensities of heavy species. The growth proceeds on to soot if the fuel/oxygen ratio exceeds the critical soot limit.

MECHANISTIC FEATURES OF AROMATICS GROWTH

Analysis of these data has provided some insights into possible mechanisms of destruction of the fuel and the formation and destruction of intermediates (3,4,6). There is indication that aromatic hydrocarbons provide a structure capable of stabilizing, by internal aromatic substitution reactions, the radicals formed from addition of aromatic radical species to non-aromatics. Specifically, it appears that the combined presence of aromatic radicals, unsaturated aliphatics such as acetylenic species and H atoms is particularly favorable to growth of PAH and soot. Therefore, the production of phenyl radical (C_6H_5) and the competition between its destruction, especially with O_2, and addition to unsaturated aliphatics are important factors in the molecular weight growth of aromatics.

With these mechanistic points in mind we return to the earlier discussion of the consumption of species immediately downstream of the peak concentration of the high molecular weight material. While the consumption is mainly by oxidation, it is accompanied by further increase in the mean molecular weight of the heavy species. Since the largest amount of material being consumed is acetylene, diacetylene, and vinylacetylene, and since these unsaturated aliphatics are identified as important species for molecular weight growth by addition reactions with aromatic radicals, one can infer that the acetylenic species do indeed contribute to the growth of the aromatic structures of which the heavy molecules and soot are comprised, presumably by addition reactions with the heavy aromatics. Aromatic species with acetylenic side groups are observed in the mass range ($\gtrsim$200 amu) where individual identifications were possible, and the amount of acetylenic species consumed in this region of the flame greatly exceeds the amount of soot eventually formed. However, the peak flux of heavy species also exceeds the amount of soot eventually formed, so the proportions of the final soot mass contributed by the acetylenic species and by the heavy aromatics are not established. Qualitatively similar behavior was observed in a sooting acetylene/oxygen flame. In both the acetylene and benzene flames, the oxidative and possibly pyrolytic destruction of heavy species occurring downstream of their peak concentration would appear to be an important source of polycyclic aromatics emitted from the flame.

FORMATION OF FIRST AROMATIC RINGS

In flames of aliphatic fuels the first aromatic rings must be formed from non-aromatic precursors. Possible mechanisms for this critical step have been assessed (7) by comparing predicted formation rates against experimental values calculated from mole fraction profiles of compounds measured in a low-pressure 1,3-butadiene/oxygen flame using the instrument shown in Fig. 2. Postulated mechanisms involving butadienyl radical (C_4H_5) reacting with an acetylenic species and followed by rapid

cyclization were found to form benzene, toluene, phenylacetylene, and styrene at rates consistent with the data. The rate-controlling steps and predicted rate constants are as follows:

$$C_4H_5 + C_2H_2 \rightarrow C_6H_6 + H, \quad \log k_1 = 8.5 - 3.7/\theta$$
$$C_4H_5 + C_3H_4 \rightarrow C_6H_5CH_3 + H \quad \log k_2 = 8.5 - 3.7/\theta$$
$$C_4H_5 + C_4H_2 \rightarrow C_6H_5C_2H + H, \quad \log k_3 = 8.5 - 1.8/\theta$$
$$C_4H_5 + C_4H_4 \rightarrow C_6H_5C_2H_3 + H, \quad \log k_4 = 8.5 - 0.6/\theta$$

where k's are in $\ell\ mol^{-1}s^{-1}$ and $\theta = 2.3\ RT$ is in kcal mol^{-1}. Aromatics thus formed could subsequently participate in molecular weight growth as discussed above.

CONCLUSIONS

The chemistry of heavy aromatic compounds in fuel-rich flames involves numerous intermediate species whose sequential formation and destruction give a progression to decreasing amounts of increasingly heavy species, leading eventually to soot if the fuel/oxygen ratio is high enough. The combined presence of aromatic radicals, unsaturated aliphatics such as acetylenic species and H atoms is particularly favorable to molecular weight growth. When the initial fuel contains no aromatics, mechanisms controlled by butadienyl radical reacting with acetylenic species can form single-ring aromatics at rates consistent with observed values.

ACKNOWLEDGEMENTS

Support from the following sponsors is gratefully acknowledged: Environmental Protection Agency, Grant No. R803242; National Science Foundation, Particulate and Multiphase Processes Program, Grant No. NSF ENG 75-22679 A01; Exxon Research and Engineering Company, Exxon/MIT Combustion Research Program; and the National Institute of Environmental Health Sciences, Center Grant No. 5 P30 ES02109-02.

REFERENCES

1. Adams, D. E.: Measurement Technique for Charged Soot Particles in Flames, Chemical Engineer's Degree Thesis, Department of Chemical Engineering, M.I.T., Cambridge, Mass. (1976).

2. Wersborg, B. L., Yeung, A. C., and Howard, J. B.: Concentration and Mass Distribution of Charged Species in Sooting Flames, Fifteenth Symposium (International) on Combustion, The Combustion Institute, Pittsburgh, pp. 1439-1447 (1975).

3. Bittner, J. D. and Howard, J. B. (1981): Pre-Particle Chemistry in Soot Formation. In: Particulate Carbon - Formation During Combustion, edited by D. C. Siegla and G. W. Smith, pp. 109-142, Plenum Press, New York.

4. Bittner, J. D. and Howard, J. B.: Composition Profiles and Reaction Mechanisms in a Near-Sooting Premixed Benzene/Oxygen/Argon Flame, Eighteenth Symposium (International) on Combustion, The Combustion Institute, Pittsburgh, pp. 1105-1116 (1981).

5. Howard, J. B. and Bittner, J. D.: Structure of Sooting Flames. In: Soot Formation in Combustion Systems and Its Toxic Properties, edited by J. Lahaye, Plenum Press, New York (1983).

6. Bittner, J. D., Howard, J. B., and Palmer, H. B.: Chemistry of Intermediate

Species in the Rich Combustion of Benzene. In: Soot Formation in Combustion Systems and Its Toxic Properties, edited by J. Lahaye, Plenum Press, New York (1983).

7. Cole, J. A., Bittner, J. D., Longwell, J. P., and Howard, J. B.: Formation Mechanisms of Aromatic Compounds in Aliphatic Flames, presented at ACS National Meeting, Seattle, Washington, March 20-25, 1983 (to be published).

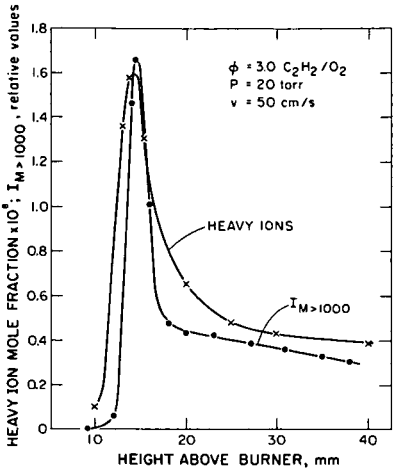

FIGURE 1. Concentration of heavy ions and signal intensity of high-mass (M>1000 amu) species in sooting acetylene-oxygen flame (ϕ = equivalence ratio; P = pressure; v = cold gas velocity).

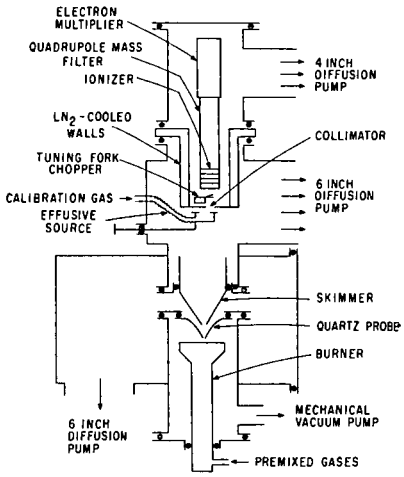

FIGURE 2. Molecular beam mass spectrometer system for the study of one-dimensional low-pressure premixed laminar flames.

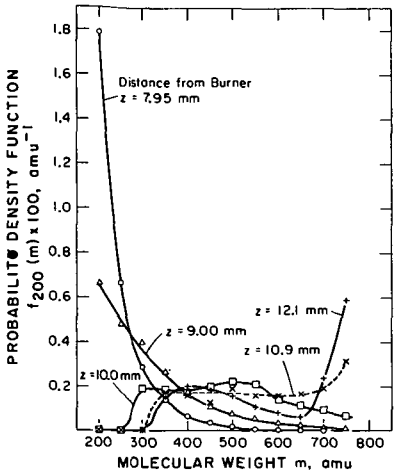

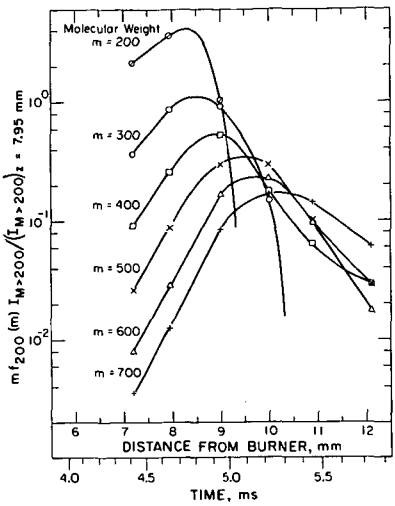

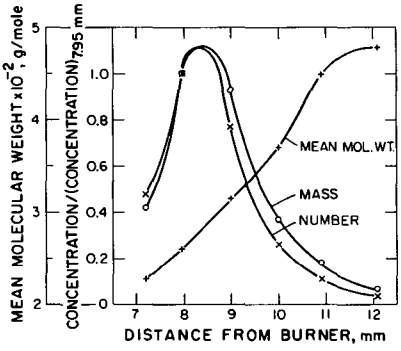

FIGURE 3. (ABOVE, LEFT) Probability density function for high-mass signal at several positions in near-sooting benzene-oxygen flame. (Pressure = 2.67 kPa; cold gas velocity = 50 cm/s; equivalence ratio = 1.8.)

FIGURE 4. (ABOVE, RIGHT) Variation with distance from burner of mass of material in molecular weight range m to m + dm at different molecular weights, normalized with number of moles of M>200 amu material at 7.95mm above burner. (Same flame as in Fig. 3.)

FIGURE 5. (BELOW) Variation of mean molecular weight and mass and number concentration of M>200 amu material with distance from burner. (Same flame as in Fig. 3.)

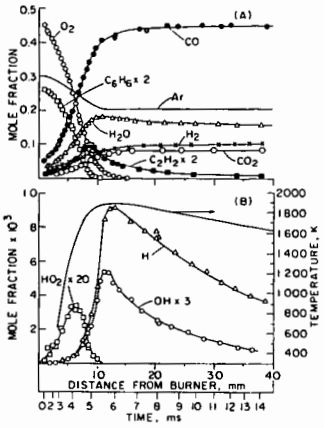

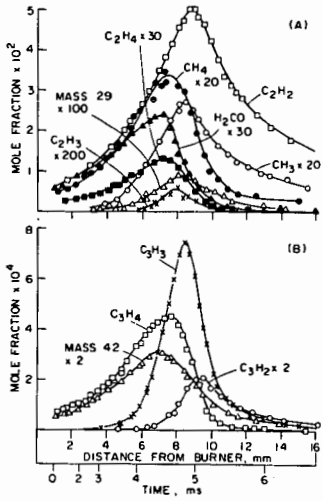

FIGURE 6. (LEFT) Mole fractions and temperature vs. distance from burner in near-sooting benzene-oxygen flame. (Same flame as in Fig. 3.)

FIGURE 7. (RIGHT) Mole fractions of species with masses between 15 and 44 amu vs. distance from burner in near-sooting benzene-oxygen flame. (A) Mass 29 may be C_2H_5 or HCO. (B) Mass 42 may be C_3H_6 or C_2H_2O. (Same flame as in Fig. 3.)

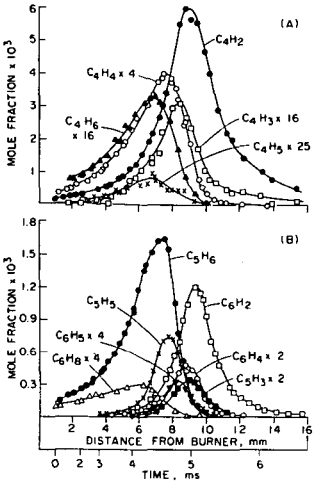

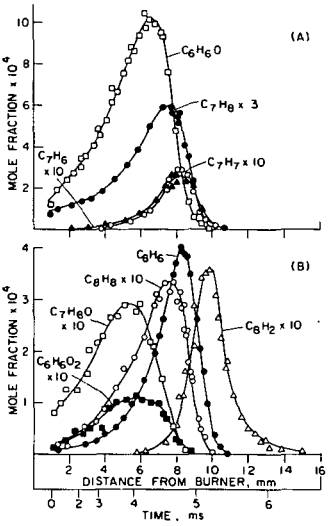

FIGURE 8. (LEFT) Mole fractions of C_4 (A), C_5 and C_6 (B) hydrocarbons vs. distance from burner in near-sooting benzene-oxygen flame. (Same flame as in Fig. 3.)

FIGURE 9. (RIGHT) Mole fractions of species with masses between 90 and 100 amu vs. distance from burner in near-sooting benzene-oxygen flame. (Same flame as in Fig. 3.)

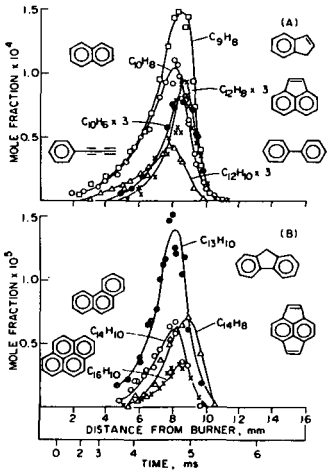

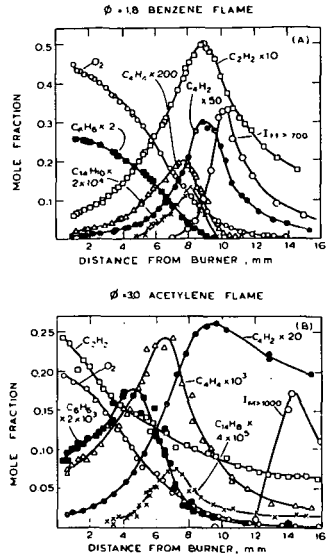

FIGURE 10. (LEFT) Mole fractions of polycyclic aromatic hydrocarbons vs. distance from burner in a near-sooting benzene-oxygen flame. (Same flame as in Fig. 3.)

FIGURE 11. (RIGHT) Mole-fraction profiles of selected compounds and signal intensity profiles of high molecular weight species for benzene-oxygen (above) and acetylene-oxygen (below) flames. [Same flames as in Fig. 3 (above) and Fig. 1 (below).]

POLYCYCLIC AROMATIC COMPOUNDS IN FLUIDIZED BED COMBUSTION OF COAL

P.M. Walsh[a], K.S. Chiu[b], J.M. Beer[a,c] and K. Biemann[b]

[a]Energy Laboratory
[b]Department of Chemistry
[c]Department of Chemical Engineering

Massachusetts Institute of Technology
Cambridge, Massachusetts 02139

Introduction

Polycyclic aromatic compounds (PAC) have been determined in the gas and particulate effluents from fluidized bed combustion of coal, lignite, and oil shale by a number of investigators. A bibliography of the reports of these investigations is contained in a paper by Chiu, Walsh, Beer, and Biemann (1983). The concentrations of PAC in the effluents are often quite low, but depend upon the combustor configuration and operating conditions. The goal of the present investigation is to develop a mechanism consistent with measured rates of formation and destruction of PAC in atmospheric pressure fluidized bed combustion (AFBC), so that a rational approach may be taken to adjustment of conditions for minimization of PAC in the effluents. PAC are determined in samples taken from the freeboard (space above the bed), rather than from the exhaust, to observe the evolution of the PAC distribution within the combustor. Mass fractions of the most abundant PAC observed in the freeboard during AFBC of high volatile bituminous coal were reported by Chiu, et al (1983). Some correlation of the rates of disappearance of PAC with particle concentration was noted by Dutta, Chiu, Walsh, Beér, and Biemann (1983). In the present paper theoretical estimates of the rates at which PAC might be consumed by heterogeneous reactions are compared with experimental rates estimated from PAC profiles determined by Chiu et al (1983).

Experimental

The PAC were determined in samples taken in the MIT AFBC Research Facility. A detailed description of the facility may be found in a report by Beér, Sarofim, Sandhu, Andrei, Bachovchin, Chan, Chaung, and Sprouse (1981). The combustor has a square cross section 0.6 m x 0.6 m and a height, from the combustion air distributor to the outlet, of 4.4 m. Previous publications describe the procedures used for sampling, separation, and identification of PAC (Chiu et al, 1983), permanent gases (Walsh, Chaung, Dutta, Beér, and Sarofim, 1982b), and bed particles (Walsh et al, 1982a; 1982b).

The AFBC was fired with Kentucky No. 9 high volatile bituminous coal crushed to minus 6.35 mm. The apparent ASTM rank of this coal was high volatile B bituminous. Other coal properties are given by Chiu et al (1983). The bed material was Reed limestone (middle ledge) crushed to minus 6.35 mm.

The experimental conditions at which the PAC were measured are listed in Table 1. In the specification of bed heights, sampling points, etc., the height above the distributor is designated by the symbol z. The top of the fluidized bed is at $z = L_f$. Axial profiles of temperature and the mole fractions of O_2, CO, NO, and CH_4 are shown in Figure 1. The freeboard temperature in this run was relatively low, due to cooling of the combustion products by heat exchanger tubes

Table 1. Experimental Data

Run Number	K10
Fraction of theoretical air:	1.01
Superficial gas velocity based on average bed temperature and pressure at z = 0:	1.20 m/s
Minimum fluidization velocity:	0.18 m/s
Fluidized bed height:	0.65 m
Calcium/sulfur feed ratio:	3.7 kmol/kmol
Solid density of bed char particles:	336 kg/m^3
Solid density of bed stone particles:	2163 kg/m^3
Freeboard pressure:	102.6 kPa
Average freeboard temperature from z = 2.0 to 3.8 m:	964 K
Average freeboard gas velocity from z = 2.0 to 3.8 m:	1.18 m/s
Mass-based geometric mean size of elutriated char particles:	72 μm
Geometric standard deviation of elutriated char particle size distribution:	1.82
Specific surface area-based geometric mean size of elutriated char particles:	60 μm
Mass-based geometric mean size of elutriated stone particles:	74 μm
Geometric standard deviation of elutriated stone particle size distribution:	2.67
Specific surface area-based geometric mean size of elutriated stone particles:	46 μm
Terminal velocity of mean size elutriated char particles:	0.012 m/s
Terminal velocity of mean size elutriated stone particles:	0.046 m/s
Sherwood numbers of elutriated char and stone particles	∿2
Total flowrate of elutriate:	0.01167 kg/s
Mass fraction char in elutriate:	0.063
Concentration of entrained char in the freeboard:	0.00169 kg/m^3
Concentration of entrained stone in the freeboard:	0.0260 kg/m^3

located at z = 0.8, 1.0, and 1.2 m. The bed material at the start of the run was fresh calcined limestone, therefore the ratio of CaO to $CaSO_4$ in the bed is much higher than would be present after sufficient time had elapsed to achieve steady bed composition.

The mole fractions of some of the PAC identified in samples taken from the freeboard at z = 1.6, 2.1 and 3.8 m are given in Table 2. These mole fractions are based on the volume of dry gas sampled. Table 2 includes all of the compounds which were identified at more than one height. The PAC mole fractions are plotted vs height above the distributor in Figure 2. Most of the profiles indicate only net destruction of PAC in the region of the measurements. There is some evidence that production of PAC is occurring in the freeboard, and a hint that there may be a peak mole fraction resulting from the combined production and consumption processes which tends to shift to longer times (heights) with increasing molecular weight (compare the profiles of naphthalene, phenanthrene, anthracene, and chrysene in Figures 2a and 2g). However, much significance cannot be attached to changes in the slopes of the profiles, because the uncertainty in the reported mole fractions is approximately +100, -50%. Pseudo-first order rate coefficients, k_{exp}, were derived from the mole fractions at z = 2.1 and 3.8 m:

$$u_o \frac{dC_{PAC}}{dz} = -k_{exp}\, C_{PAC} \qquad 1)$$

$$k_{exp} = -\frac{u_o}{z_2 - z_1} \ln \frac{X_{PAC,2}}{X_{PAC,1}} \qquad T,\ P,\ \Sigma C_j \cong \text{constant} \qquad 2)$$

The definitions of symbols may be found in the Nomenclature. The values of k_{exp} for the PAC identified at z = 2.1 and 3.8 m are given in Table 2. Lack of a strong dependence of the experimental rate coefficients on oxygen, temperature, or compound, and their tendency to increase with increasing particle concentration (Dutta et al, 1983), suggested that the PAC destruction process might be heterogeneous, with significant resistance from extraparticle diffusion.

Heterogeneous Mechanism for Destruction of PAC

The mechanism of the transformations of PAC in the freeboard gas/particle mixture is undoubtedly extremely complicated. The investigations of Bittner and Howard (1981a; 1981b) and Howard and Bittner (1983) on the reactions of hydrocarbon species in benzene/oxygen flames give an indication of the magnitude of the problems which may be encountered in the freeboard gas/particle mixture. Suppose that we neglect production of a given PAC by char devolatilization, synthesis from lighter species, or formation by degradation of heavier species; and that each PAC is degraded to non-PAC in irreversible, heterogeneous reactions with solid species S_i:

$$PAC + S_i \overset{k_{PAC,i}}{=} \text{products} \qquad R1)$$

We assume that the freeboard gas/particle mixture is in steady plug flow, and neglect axial dispersion. A rate expression based on this mechanism is:

Table 2. Polycyclic Aromatic Compounds Identified at Two or Three Heights in the Freeboard

Compound	Mole Fractions x10^9 (dry basis) z = 1.6m	2.1m	3.8m	k_{exp} (Hz)	$(\Sigma v)^b_{PAC}$ (m^3/kmol)	D_{PAC-N_2} x10^4 (m^2/s)
benzofuran	22.5	5.72[a]	.093[a]	2.9	.109	.577
naphthalene	991	324	1.40	3.8	.140	.515
benzo(b)thiophene	112	33.0	.070	4.3	.120	.548
quinoline	17.1	2.11	-	-	-	-
2-methylnaphthalene	25.6	8.81	.244	2.5	.161	.479
3-methylbenzo(b)thiophene	2.80	.10	-	-	-	-
1-methylnaphthalene	25.0	6.23	.04[a]	3.5	.161	.479
biphenyl	88.1	23.7	.182	3.4	.177	.455
ethylnaphthalene	2.95	.90	-	-	-	-
acenaphthylene	45.4	11.2	-	-	-	-
acenaphthene	2.19	.41	-	-	-	-
1-cyanonaphthalene	6.53	1.15	-	-	-	-
dibenzofuran	44.3	19.8	.108	3.6	.159	.475
methyldibenzofuran	.79	.59	-	-	-	-
9-fluorenone	10.3	2.50	.109	2.2	.195	.431
dibenzothiophene	23.8	9.49	.193	2.7	.170	.458
phenanthrene	125	64.7	.204	4.0	.190	.436
anthracene	9.53	8.43	-	-	-	-
fluoranthene	6.07	14.6	-	-	-	-
benzo(def)dibenzothiophene	2.43	7.34	-	-	-	-
pyrene	4.13	12.0	-	-	-	-
chrysene	1.09	3.42	.101	2.4	.240	.385

a. In the gas chromatographic separation this compound coeluted with another compound. The amount indicated is an estimate based on the relative intensities of peaks characteristic of the two compounds in the mass spectrum.

b. Fuller, Schettler, and Giddings (1966).

$$u_o \frac{dC_{PAC}}{dz} = - \Sigma k'_{PAC,i} C_{PAC} \qquad 3)$$

where $k'_{PAC,i}$, the effective rate coefficient for the heterogeneous reaction of PAC with solid species i, contains the sequential processes of diffusion of PAC to the surfaces of particles, and the heterogeneous reaction at the surfaces:

$$k'_{PAC,i} = \frac{\rho_i}{\dfrac{1}{\dfrac{6Sh_i D_{PAC}}{\phi_i \rho^*_i d_i^2}} + \dfrac{1}{k_{PAC,i} S_i \eta_{PAC,i}}} \qquad 4)$$

In order to evaluate this rate coefficient we require estimates of the concentration, diameter, solid density, and sphericity of each particle species, and the diffusion coefficients of the PAC.

Freeboard Particle Properties

High particle concentration is an important feature of the freeboard flow, however precise measurements of the particle concentrations are difficult. The problems arise from the facts that large particles (> 300 μm) are moving both upward and downward with distributed velocities; and that small particles (≲ 300 μm), which are moving primarily upward, have velocities which depend on particle size and density. Isokinetic sampling of the particles is therefore not possible. Concentrations of particles in the bed are usually determined from measurements of differential pressure. This technique can only be used in the freeboard at low superficial velocity when pressure fluctuations are not large with respect to the changes in pressure due to the presence of particles. This condition is usually not met during combustion measurements. An alternative, approximate method for the determination of particle concentrations has been developed in order to estimate the rates of heterogeneous reactions.

The particles are classified by their terminal velocities into two groups: large particles (terminal velocities greater than the mean gas velocity) and small particles (terminal velocity less than the mean gas velocity). The dependence of the flux of large particles on height in the freeboard is measured by catching descending particles in cups placed at several heights above the bed (Walsh, Mayo, and Beér, 1983). The concentration of large particles is estimated from the flux measurements by a method proposed by Walsh, Yokozeki, and Beér (1982). The basis of this estimate is an assumed initial velocity distribution (Gaussian) of particles leaving the bed surface. For a given particle flux at the bed surface, a given standard deviation of the velocity distribution, and the assumptions of negligible drag and total reflux; both the flux and concentration of particles at a given height are uniquely determined. In this way the large particle concentrations can be estimated from the flux measurements.

The small entrained particles are precipitated by cyclones from the exhaust, so their flux at the freeboard exit is known. By assuming that they move only upward at a constant velocity equal to the mean gas velocity minus the terminal velocity of the mean size particles, their concentration can also be estimated. Errors in this estimate may arise from:

1. Cyclone collection efficiency less than 1.
2. SO_2 and/or CO_2 reactions with stone and combustion of char in the freeboard and exhaust pipe before the collection point.
3. Refluxing of the small particles down the freeboard wall (Pemberton and Davidson, 1983).

Probably the most important problem, however, is in the initial assumption: that the particles can be divided into two groups having mean sizes independent of height. The particle size and velocity distributions undergo continuous evolution from the top of the bed (and even within the bed itself) to the combustor outlet. A more detailed calculation can be made by machine computation, but the value of such an effort is to some extent negated by the lack of experimental data with which to compare the predictions.

The mass-based particle size distributions of the stone and char particles in a sample of the elutriate precipitated in the cyclones during the present experiment are shown in Figure 3. The mass fractions of stone and char in the elutriate were calculated from the heating value of the material in each size range. The heating value of pure char was estimated using Dulong's formula with a composition derived from the ultimate and proximate analyses of the coal. The specific surface area-based mean particle sizes were calculated from the standard deviation and mass-based mean sizes (Irani and Callis, 1963). The sphericity of the entrained stone and char particles was estimated to be 0.5; their solid densities were assumed to be the same as those of the larger stone and char particles taken from the bed. Terminal velocities of the particles were calculated using the correlation of Pettyjohn and Christiansen (1948). The properties of the entrained particles are summarized in Table 1.

The refluxing particles were assumed to have the same size, sphericity, and solid density as bed particles. Specific surface area-based mean sizes of the bed stone and char particles were 780 and 2900 μm, respectively. The mass fraction of char in the bed and refluxing particles is only 0.43 wt %.

Total particle concentrations estimated in the present experiment by the approximate methods outlined above are shown in Figure 4. The bed particle concentrations were determined from measurements of differential pressure, the refluxing particles from the samples collected in the cups, and the entrained particles from the cyclone catch. An explanation of the second curve on Figure 4 is given in the Discussion section.

Molecular Diffusion Coefficients of Polycyclic Aromatic Compounds

Experimental measurements of the molecular diffusion coefficients of PAC are rare. Diffusion coefficients in air at atmospheric pressure have been reported for naphthalene and biphenyl at 298 K, anthracene at 372 K (Mack, 1925), and biphenyl at 491 K (Gilliland, 1934). Howard and Bittner (1983) determined diffusion coefficients of heavy species (W = 200 to 750 kg/kmol) from concentration profiles measured in a near-sooting benzene/oxygen/argon flame (equivalence ratio 1.8), in a region of the flame where the slopes of the species profiles, $d\ln C/dz$, were determined only by diffusion. The pressure in the flame, and the temperature in the region of the measurements were 2.67 kPa and 1800 K, respectively. Assuming that the species observed were polycyclic aromatic hydrocarbons, Howard and Bittner estimated their diffusion coefficients at 300 K from the correlation of Fuller, Schettler, and Giddings (1966), using the temperature dependence

derived from the Lennard-Jones 12-6 potential, as recommended by Sherwood, Pigford, and Wilke (1975). The approximation given by Fristrom and Westenberg (1965) to the temperature dependence of the diffusion collision integral was used. The correlation of Fuller et al, with this modification, becomes (in SI units):

$$D_{AB} = \frac{1.60\times10^{-4}\ T^{1.67}\left(\frac{1}{W_A} + \frac{1}{W_B}\right)^{1/2}}{P[(\Sigma v)_A^{1/3} + (\Sigma v)_B^{1/3}]^2} \quad m^2/s \qquad 5)$$

Howard and Bittner (1983) reported good agreement between their experimental diffusion coefficients and those estimated from the modified correlation. The discrepancies between estimated values and the experimental values for PAC reported by Mack (1925), Gilliland (1934), and Howard and Bittner (1983) are ± 10 to 15%.

Estimates of the binary diffusion coefficients of PAC in N_2 using Equation 5 are listed in Table 2. The procedure given by Fuller et al (1966) for the estimation of the molecular diffusion volumes from atomic diffusion volumes was followed. The volume increment -0.0202 m^3/kmol was added for each aromatic and heterocyclic ring, but not for the ring containing the keto group in 9-fluorenone.

Discussion

An upper limit on the rate coefficient for the surface reaction can be estimated from the product of the frequency of collisions of the PAC with unit area of a surface and the particle external surface area per unit volume of gas:

$$k_{PAC,i} S_i \eta_{PAC,i} \rho_i \leq \left(\frac{RT}{2\pi W_{PAC}}\right)^{1/2} \frac{6}{\phi_i \rho_i^* d_i} \rho_i \qquad 6)$$

Using the entrained particle properties in Table 1 the upper limits for naphthalene at 964 K are 310 and 100 Hz for the stone and char particles, respectively.

The rate coefficient for the diffusion process is equal to

$$\frac{6 Sh_i D_{PAC}}{\phi_i \rho_i^* d_i^2} \rho_i \qquad 7)$$

Using the elutriated particle properties from Table 1 and the diffusion coefficient for naphthalene in N_2 from Table 2, values of 7 and 2 Hz are obtained for the stone and char, respectively. The rate coefficient for the surface reaction is therefore estimated to be more rapid than that for external diffusion for values of the sticking coefficients greater than about 0.02. If the sticking coefficient were sufficiently large, say $\geq$ 0.1, the experimental rate coefficient would be approximately equal to the diffusion limited rate coefficient given by Equation 7.

In general the concentration of particles, ρ_i, is a function of height, as shown in Figure 4. However, the quantity $\Sigma 6 Sh_i \rho_i / \phi_i \rho_i^* d_i^2$ is dominated by the approximately constant concentration of small particles over most of the height of the freeboard under the present conditions, shown by the second curve in Figure 4. We may therefore base estimates of the diffusion limited rate coefficients from Equation 7

on the properties of the small particles alone.

The calculated rate coefficients for destruction of PAC by diffusion limited surface reactions on the small stone and char particles are plotted vs. PAC diffusion coefficient in Figure 5. The rate coefficient for simultaneous diffusion controlled destruction on both types of particles is the sum of the values shown for stone and char. The data points are the experimental rate coefficients determined from the PAC mole fractions at z = 2.1 and 3.8 m.

Any values of the experimental rate coefficients which are equal to, or less than the theoretical upper limit (sum of stone and char values) are consistent with the model. Since this condition is not difficult to satisfy the location of the experimental points below the upper limit is little more than a justification for further testing and examination of the model. However, the consistency of the data points (factor of 2) is interesting. If the similarity of the values of the experimental rate coefficients is not due to significant diffusion resistance, then the rate coefficients for the net destruction of PAC by heterogeneous and/or homogeneous reactions are rather insensitive to molecular structure. The location of the experimental points between the rate coefficients for diffusion limited reaction on stone and char is an indication that at least part of the stone is participating in the reaction. Such a conclusion is not justified however, considering the assumptions and approximations used in the model and calculations. The reaction might be occurring only on the char. If the PAC destruction were only via heterogeneous reactions the intercept of a line through the data points would be zero at $D_{PAC} = 0$. The extrapolated value is approximately 0.7 Hz.

Conclusion

A heterogeneous mechanism for destruction of PAC in the AFBC freeboard could not be ruled out by comparison with the rates of disappearance of 2 to 4 ring PAC at one set of operating conditions. If heterogeneous reactions are, in fact, responsible for PAC destruction, a more detailed model accounting for production of PAC and finite rates of the surface reactions may be needed. The relative importance of stone and char particles can only be determined by additional measurements over a range of ratios of the char/stone concentrations. The possibility that only a fraction of the surface area of each type of particle is utilized, due to nonuniform surface composition, will be difficult to assess. Better spatial resolution of the PAC profiles is needed.

Acknowledgements

This work was supported by the National Institute of Environmental Health Sciences, National Institutes of Health (Center Grant No. 5 P30 ES02109). The measurements of PAC were made in conjunction with other AFBC experiments which are supported by the Office of Fossil Energy, U.S. Department of Energy (Grant No. DE-FG22-80PC30215) and by the Tennessee Valley Authority (Contract No. TV-55783).

The authors thank Professor J.B. Howard for helpful discussions of his determination of diffusion coefficients from the flame measurements. We are indebted to Professor J.P. Longwell for his suggestion that interactions of PAC with particles might be a significant determinant of the PAC concentrations in the freeboard. The responsibility for the accuracy of the analysis, however, rests entirely with the authors. We are grateful for the assistance of James R. Byrd of the

Tennessee Valley Authority, Chattanooga, in supplying the coal, limestone, and analyses of the particle samples. We thank Ms. Bonnie Caputo of the MIT Energy Laboratory for patiently and expertly typing the drafts and final manuscript.

Nomenclature

C_j concentration of gaseous species j, kmol/m^3

d_i specific surface area-based geometric mean diameter of particles i, m

D_{AB} binary diffusion coefficient, m^2/s

D_{PAC} diffusion coefficient of PAC in the freeboard gas, assumed to be equal to D_{PAC-N_2}, m^2/s

k_{exp} experimental first order rate coefficient, Hz

$k_{j,i}$ rate coefficient for surface reaction of gaseous species j with particles i, m/s

$k'_{j,i}$ effective first order rate coefficient for heterogeneous reaction of gaseous species j with particles i, Hz

L_f fluidized bed height, m

P pressure, Pa

R gas constant = 8314 J/kmol.K

S_i BET specific surface area of particles i, m^2/kg

Sh_i Sherwood number for particles i, dimensionless

T temperature, K

u_o superficial (empty tube) gas velocity, m/s

W_j molecular weight of species j, kg/kmol

X_j mole fraction of gaseous species j, dimensionless

z height above air distributor, m

$\eta_{j,i}$ effectiveness factor for reaction of gaseous species j with particles i, dimensionless

ρ_i concentration of particles i, kg/m^3

ρ_i^* solid density of particles i, kg/m^3

ϕ_i sphericity of particles i, dimensionless

$(\Sigma v)_j$ sum of atomic diffusion volumes for molecules of gaseous species j, m^3/kmol

References

Beér, J.M., Sarofim, A.F. Sandhu, S.S., Andrei, M., Bachovchin, D., Chan L.K., Chaung, T.Z., and Sprouse, A.M., 1981, NO_x Emissions from Fluidized Coal Combustion, Final Report under Grant No. R804978020, U.S. Environmental Protection Agency, Research Triangle Park, NC.

Bittner, J.D., and Howard, J.B., 1981a, Pre-Particle Chemistry in Soot Formation, In: Particulate Carbon Formation During Combustion, D.C. Siegla and G.W. Smith, eds., Plenum Press, NY, pp. 109-142.

Bittner, J.D., and Howard, J.B., 1981b, Composition Profiles and Reaction Mechanisms in a Near-Sooting Premixed Benzene/Oxygen/Argon Flame, Eighteenth Symposium (International) on Combustion, The Combustion Institute, Pittsburgh, PA, pp. 1105-1116.

Chiu, K.S., Walsh, P.M., Beer, J.M., and Biemann, K., 1983, Polycyclic Aromatic Compounds in Fluidized Bed Combustion of Bituminous Coal, Subbituminous Coal, and Oil Shale. In: Polynuclear Aromatic Hydrocarbons: Combustion Processes, Environmental Effects, and Biochemistry, Battelle Press, Columbus, OH.

Dutta, A., Chiu, K.S., Walsh, P.M., Beer, J.M., and Biemann, K., 1983, The Rates of Methane and Naphthalene Destruction in the Freeboard of a Fluidized Bed Coal Combustor, American Chemical Society, 185th National Meeting, Seattle, WA, March 20-25, Division of Environmental Chemistry, Extended Abstract.

Fristrom, R.M., and Westenberg, A.A., 1965, Flame Structure, McGraw-Hill, NY, p. 276.

Fuller, E.N., Schettler, P.D., and Giddings, J.C., 1966, Industrial and Engineering Chemistry, 58, No. 5, 19.

Gilliland E.R., 1934, Industrial and Engineering Chemistry, 26, 681.

Howard, J.B., and Bittner, J.D., 1983, Structure of Sooting Flames, In: Soot Formation in Combustion Systems and Its Toxic Properties, J. Lahaye, ed., Plenum Press, NY.

Irani, R.R., and Callis, C.F., 1963, Particle Size: Measurement, Interpretation, and Application, Wiley, NY, pp. 43-45.

Mack, E., 1925, J. Am. Chem. Soc. 47, 2468.

Pemberton, S.T., and Davidson, J.F., 1983, Elutriation of Fine Particles from Bubbling Fluidized Beds, Fourth International Conference on Fluidization, Kashikojima, Japan, May 29 - June 3.

Pettyjohn, E.S., and Christiansen, E.B., 1948, Chem. Eng. Prog. 44, 157.

Sherwood, T.K., Pigford, R.C., and Wilke, C.R., 1975, Mass Transfer, McGraw-Hill, NY, p. 18.

Walsh, P.M., Chaung T.Z., Dutta, A., Beér, J.M., and Sarofim, A.F., 1982a, Particle Entrainment and Nitric Oxide Reduction in the Freeboard of a Fluidized Coal Combustor, American Chemical Society, Division of Fuel Chemistry, Preprints, Vol. 27, No. 1, pp. 243-261.

Walsh, P.M., Chaung, T.Z., Dutta, A., Beér, J.M., and Sarofim, A.F., 1982b, Nitric Oxide Reduction in the Freeboard of a Fluidized Bed Coal Combustor, Nineteenth Symposium (International) on Combustion, The Combustion Institute, Pittsburgh, PA, pp. 1281-1289.

Walsh, P.M., Yokozeki, A., and Beér, J.M., 1982, Unpublished work.

Walsh, P.M., Mayo, J.E., and Beér, J.M., 1983, Refluxing Particles in The Freeboard of a Fluidized Bed, American Institute of Chemical Engineers, 1983 Annual Meeting, Washington, DC, October 30 - November 4.

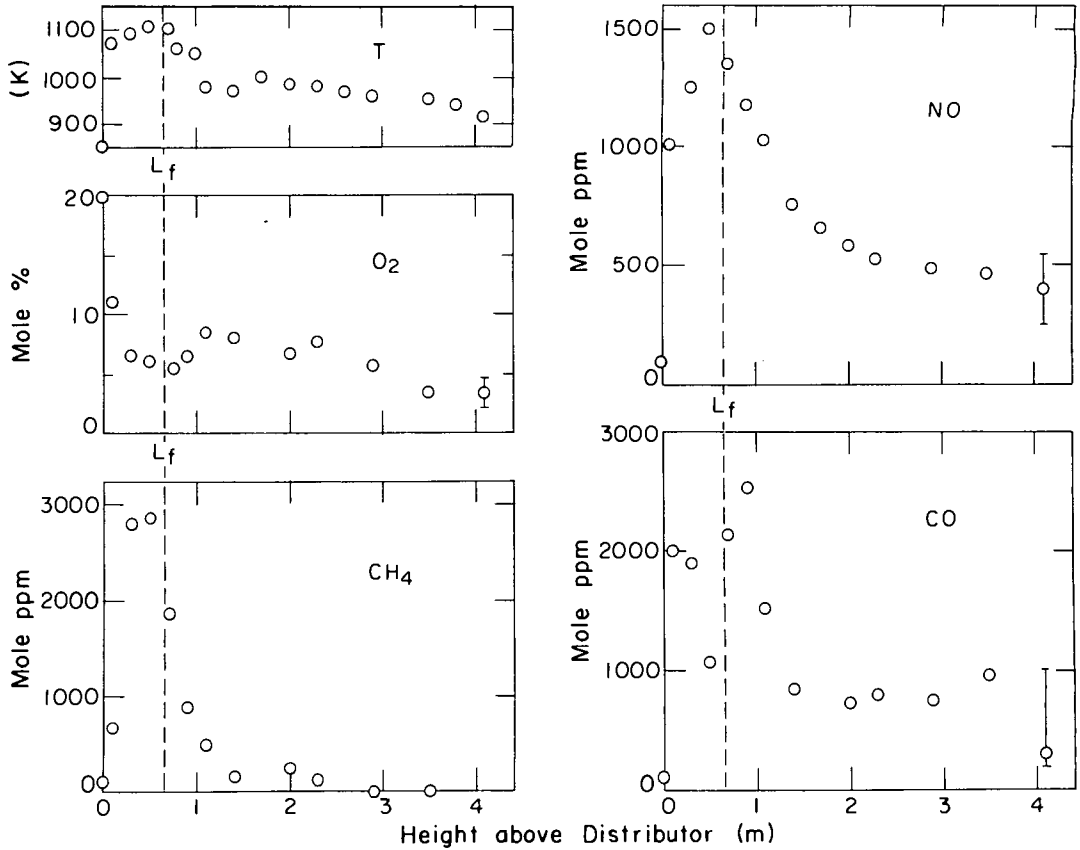

Figure 1. Temperature and mole fractions of light gaseous species (dry basis) vs. height in the bed and freeboard.

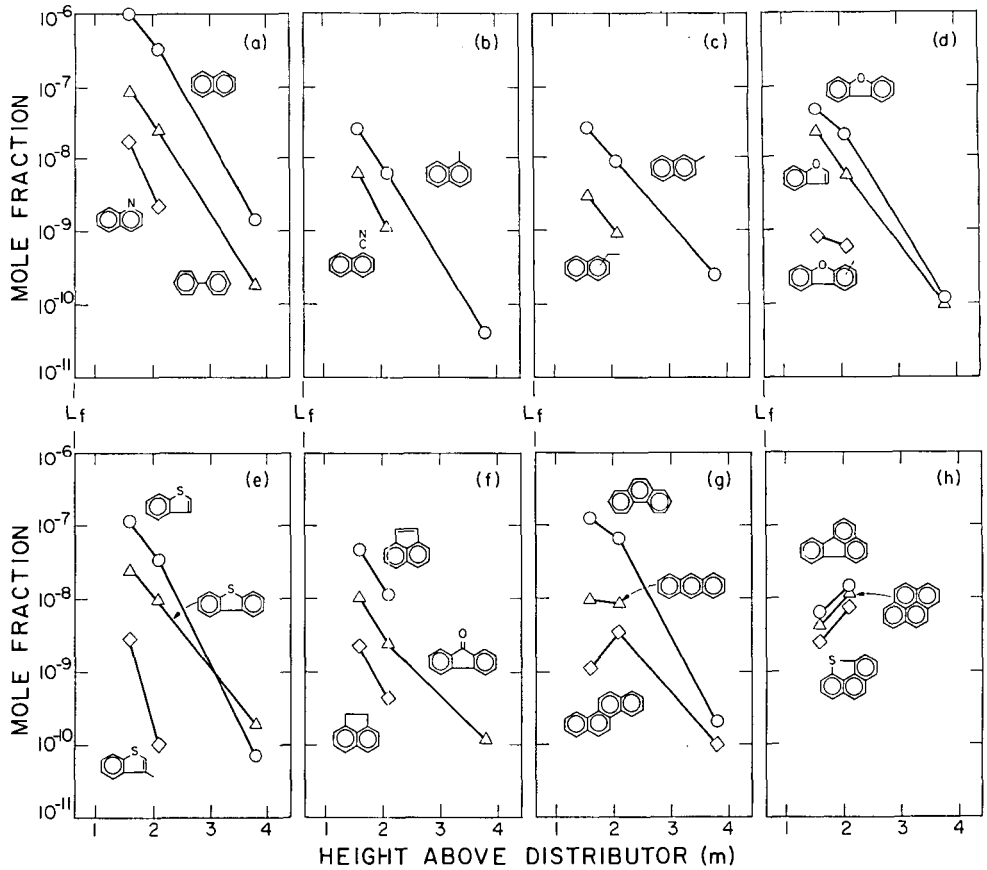

Figure 2. Mole fractions of polycyclic aromatic compounds (dry basis) vs. height in the freeboard.

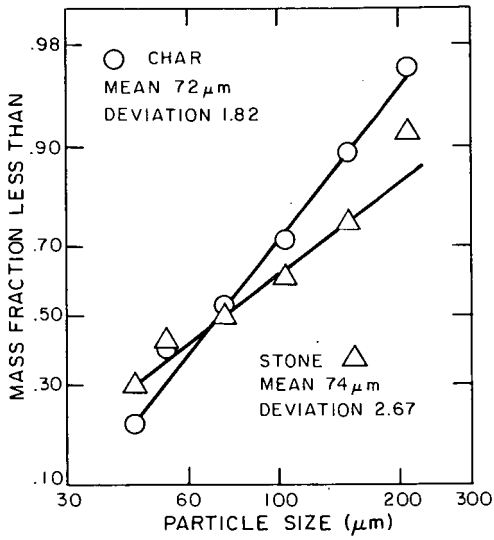

Figure 3. Size distributions of elutriated char and stone.

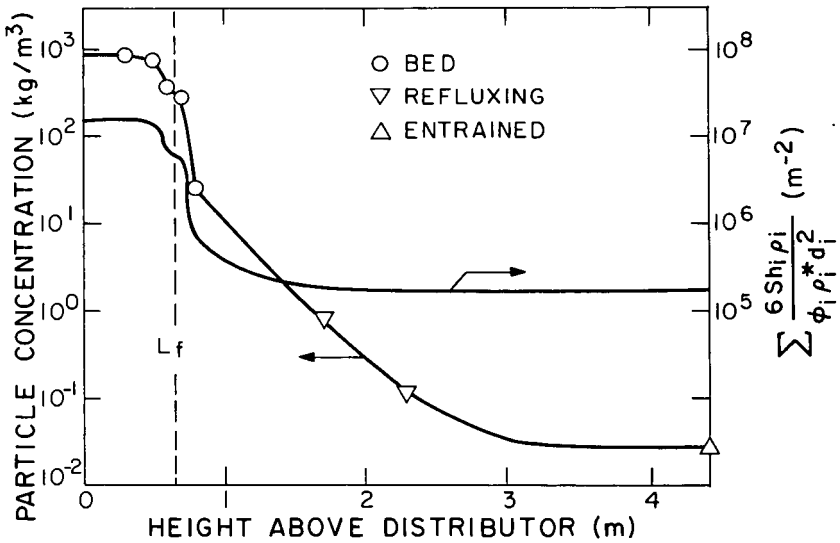

Figure 4. Particle concentration vs. height in the bed and freeboard.

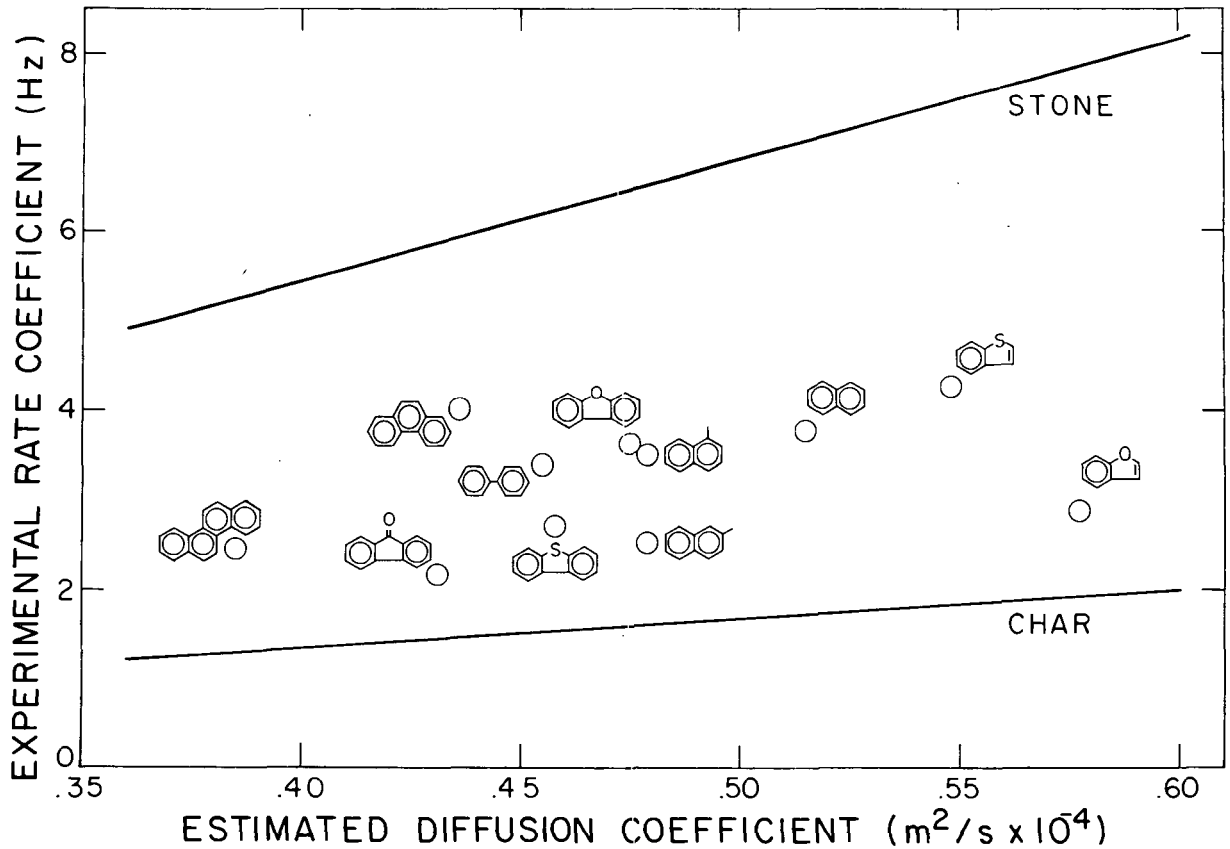

Figure 5. Experimental pseudo-first order rate coefficients vs. estimated molecular diffusion coefficients of the polycyclic aromatic compounds.

EFFECTS OF PYROLYSIS CONDITIONS ON COAL DEVOLATILIZATION

J. D. Freihaut and D. J. Seery
United Technologies Research Center
East Hartford, CT 06108

Phenomenological aspects of coal devolatilization are known to vary significantly with coal rank and the experimental conditions (1). Arrhenius rate parameters or volatile yields and product distributions can differ appreciably (2,3,4,5) for coals of similar rank depending on the experimental configuration. Differences in proposed chemical kinetic mechanisms undoubtedly account for part of the differences in reported rate parameters. However, experimentally associated variation of product yields and distributions and temperature sensitivities of global rates for similar coals implies that the observable path of the devolatilization process is the result of coupled chemical and transport processes. The physical characteristics of coal devolatilizing in a given set of conditions are also observed to vary significantly with chemical characteristics of the parent coal (6,7,8). And for a particular coal, the physical characteristics during devolatilization are observed to be a function of the conditions of heating (9,10,11,12). Such associations also imply that observable behavior during coal devolatilization is a result of the coupling between the chemical nature of the parent coal and particular conditions of the experiment.

Polycyclic aromatic hydrocarbon species represent a major fraction of the volatile yields obtained from a wide range of coals. The overwhelming majority of these species are condensible under conditions of normal temperature and pressure and are operationally referred to as coal tars. Tar yields obtained from the devolatilization of coal are sensitive functions of the chemical characteristics of the parent coal and the conditions of devolatilization. As tar yields for a particular coal are changed by variation of either the chemical characteristics of the parent coal or conditions of devolatilization, the yield structure and characteristics of the products are also changed.

The purpose of this communication is to demonstrate that progress in understanding the relative importance of chemical and physical factors in coal devolatilization is linked to progress in understanding the formation, evolution and secondary reactions of PAH species which are apparently formed within the coal particle very early in the devolatilization process. More specifically, the objectives are to demonstrate the significance of the tar formation and evolution phase of coal devolatilization in determining:

1. the yield structure of volatile products from a range of coals;

2. the change in yield structure with conditions of devolatilization;

3. the degree of coupling between chemical and physical phenomena during the main phase of mass release.

Experimental

Two experimental techniques were employed in obtaining the results - a heated grid apparatus and a flash lamp chamber. Figure 1 shows the heated grid and associated control and monitoring connections. Since the power supply driving the grid is programmable, the heating rate of the grid can be controlled by interfacing the power supply to microprocesses or circuitry. Programmed heating rates of < $1^{o}C$/sec to 10^3 ^{o}C/sec are available by use of this technique. The heated grid cell is interfaced to an infrared gas cell. The cell is coupled to an FT-IR instrument to allow immediate analysis of low molecular weight volatiles. Details of the operation of the heated grid (screen preparation, sample loading, thermocouple measurements) are given elsewhere (13,14).

The grid technique, as employed in this laboratory, cannot be used with particles less than ~ 70 μm and heating rates are practically limited to upper values ~ 10^3 ^{o}C/sec. A different technique is needed to heat particles in the 1-70 μm range at programmed heating rates of 10^5 ^{o}C/sec. To obtain these conditions of large thermal flux/particle diameter ratios a flash lamp assembly replaces the heated grid chamber of Fig. 1. In this technique the inside of a pyrex or quartz tube is dusted with the coal. The tubes are 2.5 cm in diameter and ~ 10 cm long and sealed at one end. The coated reactor tube is placed inside a helical Xenon flash coil. The flash intensity delivered to the reactor tube is varied by the energy stored in the 1125 μf capacitor bank attached to the flash lamp. Since the total energy stored in the capacitor system is $\frac{1}{2}CV^2$, an increase in voltage from 1.5 to 2.5 kV represented approximately a 2.8 increase in flash energy output. Since the discharge time and reactor geometry remain constant the increase in programmed voltage represents an increase of 2.8 in radiation flux delivered to the reactor chamber. Pyrex reactor chambers were employed in most tests to avoid UV-induced secondary reactions. Sample sizes range in value from 3-10 mg.

Coal Characteristics

The location of the samples on a H/C vs. O/C plot are shown in Fig. 2. Figure 3 displays changes in functional group absorption characteristics as a function of rank. In general, an increase in rank is associated with an increase in the resolution of the aromatic -H bending (680-920 cm^{-1} region) and aromatic -H stretching (3000-3100 cm^{-1}), a decrease in the hydroxyl -H assoicated absorption in the 3100-3600 cm-1 region, and a maximum in aliphatic -H absorption modes 2600-3000 cm^{-1} and ~ 1400 cm^{-1} regions for hv bituminous coals. It should be noted that these functional group spectra were obtained by <u>artificially</u> establishing a baseline. A chord is drawn through the local spectra absorption minima at ~ 3600 cm^{-1} and 2000 cm^{-1}. The so-called "background" absorption beneath this chord line and the raw spectra, zero absorbance line is subtracted, leaving the chord line as the new zero absorbance line. Although this is a convenient method for comparing changes in functional group appearance, it ignores the substantial changes in optical density of coal with rank.

Figure 4 shows the background absorption subtracted in this manner as a function of carbon percentage content of the coal samples. Figure 5 shows the remaining

integrated absorption area (400-4000 cm^{-1}). This is the absorption area assumed to be associated with specific functional group characteristics, the area between the chord drawn baseline and the absorption curve. Inspection of Figs. 4 and 5 indicates that as the functional group absorption characteristics of coal decrease, its amorphous background absorption sharply increases. The underlying cause of the background absorption are not well understood. Some investigators relate such optical attenuation to particle scattering effects in the halide matrix (15,16). Others attribute the bulk of this absorption to photoabsorption by condensed aromatic ring species in the coal sample (17,18,19,20). The greater the aromaticity of the coal the greater the photoabsorption effect, that is, the greater the background absorption. The two phenomena are undoubtedly coupled via the complex refractive index for a particular coal relative to the halide matrix. The strength of coupling remains to be quantified. Overall, the total optical density of a coal is a strong function of rank as measured by $\%C_{(daf)}$.

Within the hv bituminous coals, the Western bituminous coals, although similar in elemental composition to some interior and Appalachian province coals, show absorption characteristics indicating a lower degree of aromaticity. This is indicated by the ill resolved aromatic -H absorption modes (680-920 cm^{-1} and 3000-3100 cm^{-1}) and the lower background absorption than the other bituminous coals.

As noted below, the degree of aromatic ring condensation has a substantial influence on the maximum PAH yields obtainable from a coal as well as the sensitivity of the yield to changes in pyrolysis conditions.

Tar Evolution: Coupling Between Coal Characteristics and Moderate Heating Rates

Figure 6 displays the mass fraction of dry coal evolved as volatiles for the range of coals investigated and at the heating conditions indicated. At these conditions, total yield is essentially independent of rank characteristics through high volatile bituminous coals. However, as Figs. 7 and 8 indicate, the tar yield is a sensitive function of rank characteristics of a coal. Appalachian and Interior province high volatile bituminous coals give highest yields of tars and, with the exception of a medium volatile bituminous coal, display the greatest fraction of volatiles evolved as condensible PAH species. Figure 9 indicates the variation in tar yields with heating conditions for a Western bituminous coal. There is little change in volatile yields with heating conditions for final temperatures beyond 700° C in the time period of this experiment. However, the fraction of volatiles evolved as tar decreases significantly with changes in programmed heating rate from 150° C/sec to ~ 1000° C/sec. Tar yields from Appalachian and Interior province bituminous coals yield tar species which are much less sensitive to changes in programmed heating rates. Such coals show less than 10% change in tar yield with changes in programmed heating rate in the 100-1000° C/sec range, whereas tar yields from subbituminous and Western bituminous coals can vary by as much as 50% over this range. The aromaticity, and, consequently the chemical and thermal stability of the mix of molecular components in the parent coal has a great deal of influence on the tar evolution properties of a coal.

The tar evolution potential of a coal is also observed to have a significant influence on the temperature trajectory of the heated grid in immediate contact with the

coal sample. Figure 10 shows the effect which tar evolution properties of a coal can have on a programmed temperature trajectory in low pressure conditions.

Figure 11 shows the time resolved associated between the low pressure evolution of the tar component of the volatiles and the warp in the programmed temperature trajectory. Figures 9 and 11 indicate that in low ambient pressure conditions the formation and evolution of PAH species precedes significant light gas evolution. To verify the relative release times, high speed films of the tar release process were made.

Frame-by-frame inspection of these films were compared to the rapid scan infrared data and real time pressure and temperature data. For the coals examined in this manner.

1. The initial temperature deviations are closely associated with the tar formation and release.

2. The onset of the tar release precedes the onset of the major light gas release.

3. The light gas evolution occurs mainly in the secondary temperature rise.

4. Rocky Mt. province high volatile bituminous coals displayed more overlap in the tar and light gas evolution than the Appalachian province high volatile bituminous coals.

5. Lower rank coals gave increasingly greater degrees of overlap between the light gas and tar evolution phases of devolatilization.

Dependence of Coal Nitrogen Evolution on Tar Evolution Characteristics

For final temperature < 1000°C and heating rates 10^2-10^3 °C/sec, the distribution of coal nitrogen in the tar, char or light gases produced by devolatilization is dependent on the chemical characteristics of the coal in a manner analogous to the distribution of coal mass as tar. char or light gas. An increase in the tar fraction of the volatiles with increase in aromaticity of the parent coal results in a proportionate increase in coal nitrogen in the tar. A decrease in tar yield for a particular coal by increases in apparent heating rate results in a proportionate decrease in coal nitrogen evolved as tar. As the tar yield decreases, the tar nitrogen is primarily evolved as HCN. The coupling between the tar and gaseous evolution of the coal nitrogen and the dependence on aromaticity of the parent coal are illustrated by Figs. 12-14. Mass balance details and distributions for other coals are given elsewhere (21).

Effect of Low and High Programmed Heating Rates

Table I displays the sizable variation in solids and tar yields with programmed conditions of heating for two hv bituminous coals. Inspection of Table 1 indicates tar

TABLE 1

VARIATION OF CHAR AND TAR YIELDS WITH HEATING RATES

Coal	Programmed Heating Rate (^{o}C/sec)	Wt% Char/Soot	Wt% Tar (THF Soluble)	Final Temp. ^{o}C
Utah Bit.	1	63	10	800
	10^2	53	30	800
	10^3	51	17	900
	$+10^5$*	76†	14	**
Ken Bit.	1	62	15	800
	10^2	52	39	800
	10^3	50	35	900
	$+10^5$*	61†	21	**

*Flash lamp operated at 2.5 kV-1125 μf discharge conditions, 2 msec flash pulse Particle size range of coal -140+325 mesh in all runs.

**Not known.

†A fraction of non-THF soluble tars has soot-like physical characteristics.

yields and char yields are minimized for hv Bit coals in moderate heating conditions and low pressure conditions. Very low heating rates and very high heating rates have the effect of decreasing tar yields while increasing solids yields, either in the form of char or a combination of char and soot. Light gas yields reflect the thermal flux conditions in the tar formation and evolution stages.

Summary and Discussion of Results

The formation and evolution of PAH species in coal devolatilization is observed to be a sensitive function of the mix of molecular species present in the parent coal. Through high volatile bituminous coals and within moderate heating conditions, PAH yields increase with apparent aromaticity of the coal. Those coals having the greater aromaticity, as indicated by infrared absorption characteristics, give consistently greater tar yields than less aromatic samples. Such coals also show less variation in tar yields with changes in heating rate. For moderate heating rates to final temperatures less than 1000° C, the coal nitrogen evolution mirrors the parent coal evolution as char, tar or light gas species on a mass fraction basis. Heating rates of 1° C/sec or less are observed to lower tar yields of bituminous coals while increasing char and light gas yields. On the other hand, programmed heating rates of 10^{5}-10^{6} ^{o}C/sec also result in a decrease in tar yields with an increase in solid species products. A fraction of these solids appear to be soot particles. Gaseous yields of coals subjected to such high thermal fluxes show C_2H_2, CO, CH_4, HCN, C_2H_4 and polyacetylenes as the predominant gas phase species.

Not only do tar yields vary with heating conditions but evolution times vary significantly as well. Tar formation and evolution times are observed to be of the order of several milliseconds in the highest programmed heating rates employed to fraction of seconds to seconds in moderate heating rate conditions, and hundreds of seconds in the lowest heating rates employed. Formation of polycylcic aromatic species appears to begin at relatively low temperature, that is in the 300-475° C temperature range. The ultimate tar yield than appears to be a complex function of heat and mass transfer parameters as well as chemical characteristics of these primary tars. For hv Bit coals and lower ranks, the more aromatic the primary tars, the less secondary chemical reactions influence observable behavior. For these coals, the initial mass loss of the coal is likely heat and mass transport limited. For higher rank coals, the primary tars are likely to be of such molecular weights and dimension that secondary char-forming reactions will become competitive with the tar evolution process. In view of such considerations, the wide variation in reported results reflect the coupled effects of intrinsic and extrinsic parameters on primary PAH formation and evolution.

Low heating rates allow secondary char-forming reactions of tars to take place within the coal particle. Very high heating rates introduce secondary cracking and ring condensation reactions of primary tars as they evolve. The susceptibility of primary tars to undergo char-forming or cracking reactions is a fraction of chemical characteristics of the primary tars. As noted in the Introduction the development of a comprehensive model of coal devolatilization/pyrolysis for a single rank of coal in a range of conditions or a range of coals in a single condition is contingent upon fundamental studies of the formation and evolution of primary PAH species.

REFERENCES

1. Howard, J. B., "Fundamentals of Coal Pyrolysis and Hydropyrolysis," Chemistry of Coal Utilization, 2nd Supp. Volume, M. A. Elliott (Editor), Wiley - Interscience, New York, 665 (1981).

2. Solomon, P. R. and Colket, M. B., Seventeenth Symposium (International) on Combustion, The Combustion Institute, Pittsburgh, PA, 131 (1979).

3. Anthony, D. B., Howard, J. B., Hottel, H. C. and Meisner, H. P., Fifteenth Symposium (International) on Combustion, The Combustion Institute, Pittsburgh, PA 1303 (1975).

4. Tyler, R. J., Fuel, 59, 218 (1980).

5. Kobayashi, H, Howard, J. B. and Sarofim, A. F., Sixteenth Symposium (International) on Combustion, The Combustion Institute, Pittsburgh, PA 411 (1977).

6. Brown, H. R., Hesp, W. R., and Waters, P. L., J. Inst. Fuel, 130 (1964).

7. Cameron, A. R. and Botham, J. C., Coal Science, 55, 564 (1966).

8. Habermehl, D., Orywal, F., and Beyer, Hans-Dieter, "Plastic Properties of Coal," Chemistry of Coal Utilization and Supp. Volume, M. A. Elliott (Editor), Wiley-Interscience, New York, 317 (1981).

9. Gryaznov, N. S., Coke Chem. USSR, 1, 5 (1962).

10. Van Krevlen, D. W., Huntjens, F. J., and Dormans, H. N. M., Fuel, 35, 462 (1956).

11. Kreulen, D. J. W., Fuel, 29, 112 (1950).

12. Nadziakiewicz, J., Fuel, 37, 361 (1958).

13. Freihaut, J. D., Zabielski, M. F. and Seery, D. J., Amer. Chem. Soc. Div. of Fuel Chem., 27, No. 2, 89 (1982).

14. Freihaut, J. D., Zabielski, M. F. and Seery, D. J. Nineteenth Symposium (International) on Combustion, The Combustion Institute, Pittsburgh, PA, 1159 (1982).

15. Bergmann, G., Husk, G., Karwell, J. and Luter, H., Brennstoff Chem., 35, 175 (1954).

16. Duyckaerts, G., The Analyst, 84, 201 (1959).

17. Friedel, R. A., Fuel, 38, 541 (1959).

18. Kmetko, E. A. Phys. Rev, 82, 456 (1951).

19. Brown, J. K., Jr. Chem. Soc., 744 (1955).

20. Friedel, R. A., and Queiser, J. A., Jr. Anal. Chem., 28, 22 (1956).

21. Freihaut, J. D., and Seery, D. J., Am. Chem. Soc. Div. of Fuel. Chem., 26, No. 3, 18 (1981).

ACKNOWLEDGMENTS

The authors express their gratitude to G. Wagner and D. Santos for their technical expertise in performing this investigation. Part of this work was sponsored by DOE Contract DE-AC21-81MC16221.

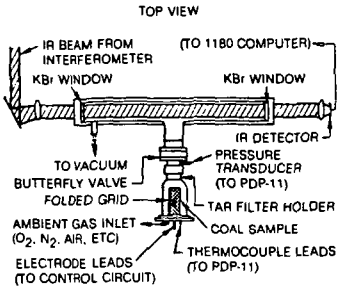

FIG. 1. Schematic of coal/devolatilization apparatus.

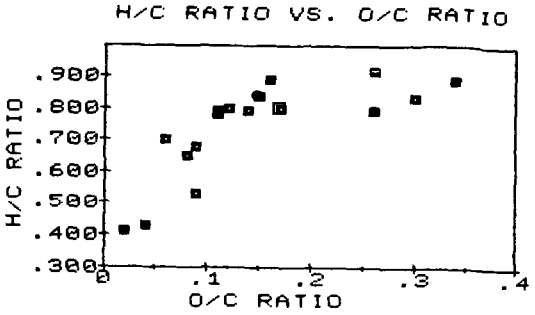

Fig. 2. Sample locations on coalification band.

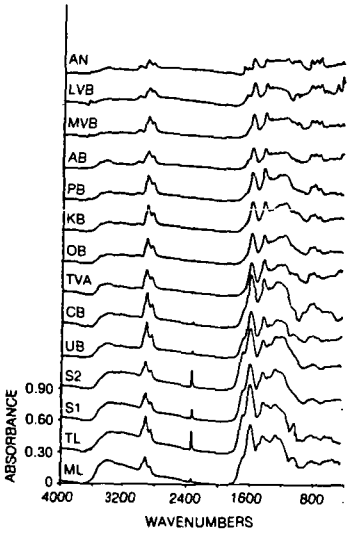

FIG. 3. Infrared absorption spectra of coals. Mineral matter subtracted · Baseline corrected.

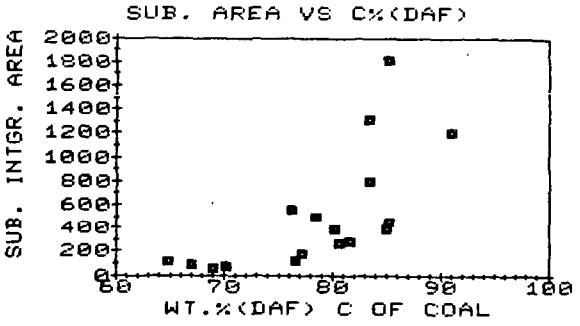

Fig. 4. Integrated area (400-4000 cm^{-1}) beneath chord drawn through tangent points at 3600 cm^{-1} and 2000 cm^{-1} and zero absorbance line: C fraction calculated dry and free (DAF) basis.

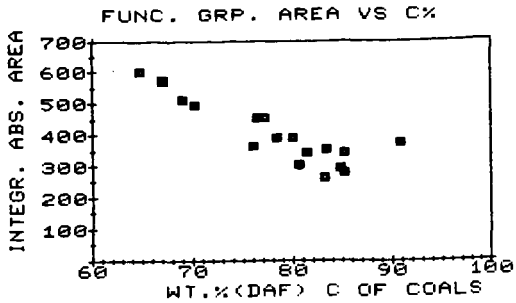

Fig. 5. Integrated area (400-4000 cm^{-1}) between chord baseline and absorption curve.

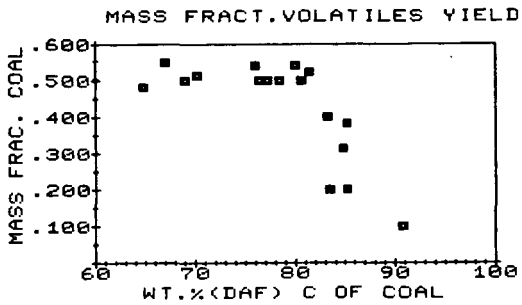

Fig. 6. Programmed heating rate 500° C/sec; final temperature 900° C; see Ref. 13, 14 for sample loading conditions; dry sample used as basis of calculation; ambient pressure ~ 10^{-2} torr; -140+325 mesh particles.

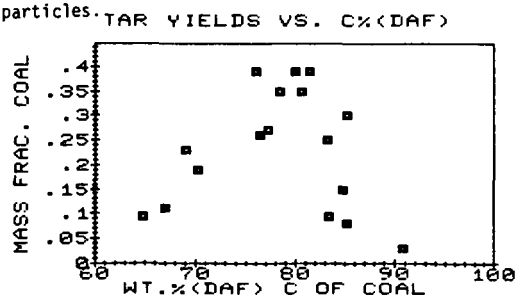

Fig. 7. Conditions as noted in Fig. 6.

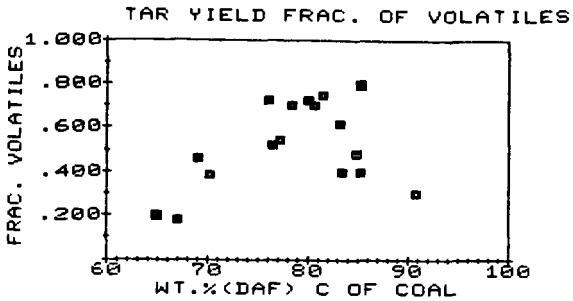

Fig. 8. Fraction of total volatiles evolved as PAH species.

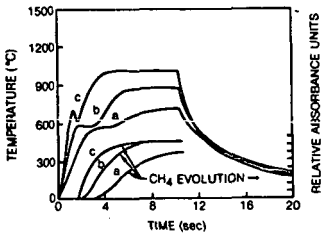

Fig. 9. Time resolved temperature and CH_4 evolution data for Rocky Mt. bituminous coal; a = 55.4% char; 30% tar; b = 52.6% Char, 24.0% tar; C = 51.3% char, 17.0%.

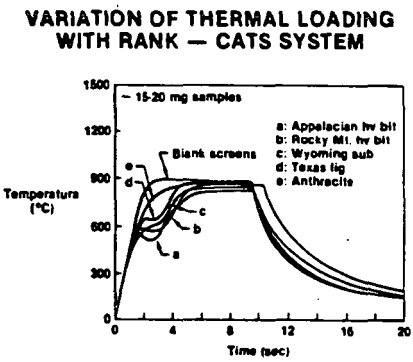

Fig. 10 a = 39% tar; b = 24% tar; c = 20% tar; d = 11% tar; c = 3% tar; see Ref. 13, 14 for loading conditions and thermocouple placement.

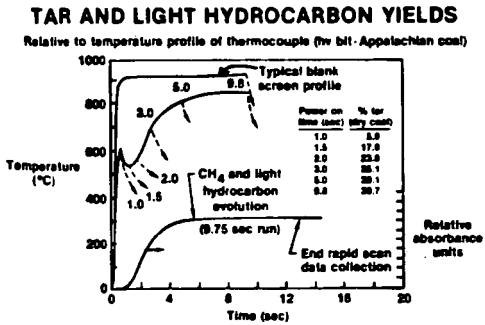

Fig. 11. Effect of tar release on temperature profile; see Ref. 13 and 14 for leading technique and thermocouple placement.

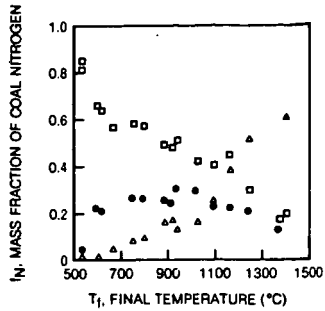

Fig. 12. Nitrogen distribution in devolatilization products; Rocky Mt. bituminous coal; ◻ = char; ● = tar; Δ HCN.

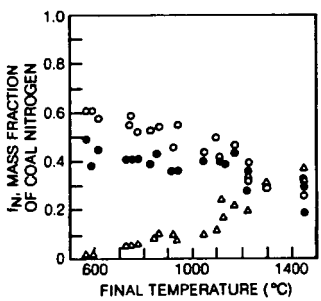

Fig. 13 Nitrogen distribution in devolatilization products; Appalachian Province bituminous coal; O = char, ● = tar, Δ= HCN.

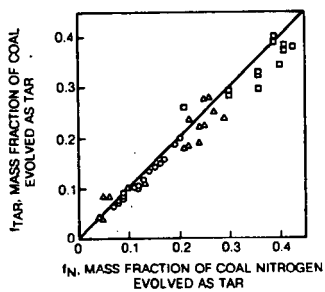

Fig. 14. Mass fraction parity between evolved tar and coal nitrogen as tar; Δ = Rocky Mt. Bit; ◻ = Appalachian Bit; O = Subbituminous.

Internal and External Mass Transfer Limitations in Coal Pyrolysis

Phillip E. Unger*
Dept. of Chem. Eng., Carnegie-Mellon University, Pittsburgh, Pa. 15213

Eric M. Suuberg
Division of Engineering, Brown University, Providence, R.I. 02912

Introduction

The recent work of Professor Howard and colleagues at MIT has helped focus attention upon the significant role that mass transfer limitations can play in shaping the pyrolysis behavior of coals (see, for example, the review by J.B. Howard, 1981). Despite having learned a great deal from these and earlier studies, it is fair to say that much remains to be learned on this topic. The present paper outlines some recent results of relevance. The focus here will be mainly on studies of high heating rate pyrolysis of finely ground coals (less than a millimeter in diameter) in low particle concentration environments. Such conditions of course exist in an enormous variety of coal conversion processes. The present focus is narrowed further by considering only the tar products of pyrolysis. Not only are these species central in discussions of mass transfer limitations, but they are of considerable interest as dominant products of most coal pyrolysis processes. Also, the topic of tar chemisty fits in well with Professor Howard's own discussion in this session, since tars have been suggested as key intermediates in certain soot formation processes during combustion of coal (Seeker et al., 1981; Mclean et al. 1981).

Background

It is customary to explore for internal mass transfer limitations in gas-solid reaction systems by performing experiments at various particle diameters. Unfortunately, data on the variation of pyrolysis product yields with particle diameter are often influenced by unintentional variations in heat transfer conditions (J.B. Howard et al., 1981). In addition, even in situations in which heat transfer to particles is relatively well defined (as in the heated wire mesh technique described below), there are sometimes difficulties in particle size characterization, since particles soften, swell, and/or flow on the surface of solid supports during pyrolysis. Consequently, most reliable information on mass transfer effects during rapid pyrolysis of fine particles has come from experiments in which the primary variable is external gas pressure.

It is well established that pyrolysis of coals under reduced pressures leads to increased volatile matter yields, compared to pyrolysis under atmospheric pressure (H.C. Howard, 1945, 1963; Anthony and J.B. Howard, 1976; J.B. Howard, 1981). There also remains little question that an increase in tar yield is mainly responsible for this increase in volatile matter yields (see above reviews and Suuberg et al., 1979a). Tar

* Present Address: Shell Development Corp., Houston, Texas

is here crudely defined as any room temperature condensable products of pyrolysis; water is excluded, but small amounts of product that is sometimes categorized as "oil" may be included. The increase in tar yields under reduced pressure has been qualitatively explained in the following terms. When heated, the coal "depolymerizes", yielding tar-like species. If these species are quickly transported away from the particle, they are observed as part of the tar products of pyrolysis. If, however, the species are given long times in the hot environment of the particles, they may be "repolymerized" into the mass of the particle, and later be counted in with the char.

While there is little debate over this qualitative picture, the development of quantitative models has revealed a great diversity of opinion concerning the nature of volatiles transport. Some have modeled the controlling transport processes by use of empirical external mass transfer coefficients (Anthony et al.,1974; Reidelbach and Summerfield,1975), some by postulating internal pore transport to be limiting (Russel et al.,1979; Melia and Bowman,1982, the latter allowing for bubble formation), one by considering nucleation and motion of bubbles within softened coal particles (Lewellen,1975) another by considering the motion of volatiles in pseudo-bubbles (not accounting for particle swelling, James and Mills, 1976), and some by employing both a crude model of pore diffusion and an external film coefficient (Chen and Wen, 1979). Other models have more explicitly considered how product compositions may vary during pyrolysis. Of these, several have represented gas film diffusion as controlling, much as in classic droplet evaporation models (Suuberg et al.,1979b; Unger and Suuberg,1981; and Zacharias,1979). In other cases, pore transport models have again been developed (Gavalas and Wilks,1980; Cheong,1977). Finally, in one case, mass transport limitations have been handled through the use of a pseudo-chemical kinetic model (Solomon and Colket,1979).

It is apparent that there continues to be considerable disagreement as to the true nature of mass transfer limitations which are responsible for the observed effects of pressure. Part of the disagreement concerns the location of the main transport limitation- whether it is internal or external to the pyrolyzing coal particle. Another source of the apparent disagreement between different workers concerns the nature of the starting coal- whether it is softening or non-softening (in the former case, it makes more sense to model the particle as essentially a droplet). In this paper, some of these issues are readdressed in the context of newly available data on the nature of coal tars.

General Observations Concerning Mass Transfer Limitations During Pyrolysis

There is a paucity of information concerning the effect of pressure on product yields observed during pyrolysis. Figure 1 presents an attempt at summarizing the majority of relevant data concerning pressure effects on tar yields during pyrolysis. It is a plot of reported tar yield vs. pressure, which illustrates the general feature of decreasing tar yield with increasing pressure. In order to compare the results for a wide range of ranks in a single figure, the data for

each coal have been "normalized" by dividing tar yield at a particular pressure by the maximum tar yield which can be obtained with that coal. This maximum tar yield naturally occurs at the lowest pressure examined during the series of experiments on the particular coal. Table 1 summarizes the conditions under which the data in Figure 1 were obtained. Where actual tar yield data were not available, a correlation based on all the available tar yield data was used to estimate normalized tar yields from weight loss data. This correlation was of form:

$$\text{Normalized tar yield} = 1 - 0.55((v_0 - v)/(v_0 - v_H))$$

where v_0 is the weight loss at the lowest pressure employed in the study, v_H is the weight loss at the highest pressure employed in the study, and v is the actual weight loss at the pressure of interest.

A rather consistent trend of decreasing tar yield with increasing pressure is observed in Fig.1. Note that the data include both softening coals and non-softening coals, ranging in rank from lignite to low volatile bituminous. It is noteworthy that the points which seem to fall above the general trend are mainly those which were normalized with respect to 0.1 atm tar yield data. Both the data of Anthony et al.(1974) and Arendt and van Heek(1981) imply that 0.1 atm is still a high enough pressure such that an additional decrease in pressure might tend to increase tar yields further; thus the normalization factor applied to the data of Arendt and van Heek(1981) and Gavalas and Wilks(1980) might be relatively higher than that applied to the other data. Were lower pressure data available in these latter two cases, it is possible that normalization with respect to such data would pull these groups' results into even better agreement with the general trend.

On the basis of the general agreement between the diverse sets of data shown in Fig. 1, it might be concluded that the effect of external pressure is similar in all ranks of coal. Of course the coals that produce the largest amounts of tar are likewise those whose product yields are most sensitive to variations in pressure. The actual nature of the mass transfer process responsible for such behavior is still unknown, however. Some order of magnitude analyses have been advanced to eliminate a few possibilities.

If a particle is non-softening and ordinary gas phase diffusion were solely responsible for transport of tar, Russel et al.(1979) have pointed out that internal pore diffusion would almost certainly be controlling. It is possible that either pressure driven bulk flow or Knudsen diffusion might play a role in pore transport (though it must be recalled that the latter does not depend upon pressure). Niksa(1981) concludes that bulk flow must control flow out of the pores, so long as the particle retains its identity as a solid; however, the possible role of an external gas film limitation is not considered.

If the coal particle softens, Attar(1978) has proposed that a competition exists between liquid phase diffusion and bubble nucleation within particles. While plausible, it seems equally likely that bubbles are formed by gas pressure swelling pores originally present within the particle. It is not clear how important bubble transport of tar species is. A small bubble breaking the surface of the particle only serves to increase the surface area of the particle slightly, but a large bubble swelling the particle into a cenosphere increases its surface area

enormously. The extent to which bubbles aid in diffusion of species from bulk to surface is also unclear. In addition, it is possible that bubble growth and motion could be a source of internal mixing. It is difficult to make any general statements about the effect of bubbles or their significance, except that it is likely that their presence will enhance transport rates. The remainder of the discussion on transport in the case of softening coals will disregard the role of bubbles.

Softened coal particles have been previously viewed as analogous to multicomponent liquid droplets (Unger and Suuberg,1981). Consider the ratio of characteristic time for internal liquid phase diffusion of tars from the bulk to the particle surface (t_i) to the characteristic time for external diffusion of the tar through a stagnant vapor film which surrounds the particle (t_e):

$$t_i/t_e = D_v C_v y/D_L C_L x$$

where D_v and D_L are vapor and liquid diffusivities,respectively; C_v and C_L are vapor phase and particle phase molar densities; y is the vapor phase mole fraction of a tar species at the particle surface,and x is the liquid phase mole fraction of a tar species at the particle surface. By use of Raoult's Law, if P^0 is the vapor pressure of the tar species, $y/x=P^0/P_{tot}$. In the case of atmospheric pressure pyrolysis, P_{tot} is 1 atm. and (C_v/C_L) is of order 10^{-2} to 10^{-3}. Neither P^0 nor D_v/D_L is known a priori. In particular, D_L is difficult to estimate, even to an order of magnitude.

It has been suggested that D_L can be estimated by use of the Stokes-Einstein equation to be of the order of 10^{-14}sq.cm/sec (Gavalas,1982). Unfortunately, such estimates are based on having a knowledge of coal viscosity, which is itself unknown to even an order of magnitude under the high heating rate, high temperature conditions of interest here. In addition, recent measurements of the diffusivity of naphthalene in high viscosity oils have shown the Stokes-Einstein equation to be invalid (Hiss and Cussler,1973). This is not surprising, since this equation has been derived assuming a large disparity in the size of solvent and solute, a condition which is met in neither coal melts nor the experiments described above. Although it is impossible to make even a crude estimate of D_L, it is reasonably certain that it will be smaller than 10^{-5}sq.cm/sec, implying that (D_v/D_L) is larger than 10^5 or 10^6. Hence, unless P^0 is of order 10^{-3} or less, internal diffusion will definitely control.

Again, P^0 is difficult to estimate, because there exist no vapor pressure data for the type of coal tars of interest. To make a crude estimate, we have improved a previously used (Suuberg et al.,1979) simple correlation for vapor pressures of high molecular weight hydrocarbons:

$$P^0(atm) = 5756*\exp(-255*MW^{0.586}/T)$$

where MW is molecular weight and T is temperature in K. See Table 2 for a comparison of the predictions of the correlation to vapor pressure data. Note that the correlation does not include any structural information, nor has it been tested against data on high molecular weight materials with significant heteroatom contents. Considering "typical" tar molecular weights in the range 500 to 2000 (Unger and Suuberg,1983a), at temperatures around 1000K, then apparently P^0 is of order 10^{-1} to 10^{-6} atm. On the basis of this range of values, it is impossible to draw a firm conclusion regarding the relative importance of internal and external mass transfer limitations. It is possible that

the escape of light species is limited by internal diffusion rates, but the escape of heavy species is limited by external film diffusion.

In this paper, we explore some new experimental evidence which sheds some light upon the nature of the transport limitations which exist during coal pyrolysis. Other important aspects have been presented elsewhere (Unger and Suuberg,1983a,1983b).

Experimental

Data will be presented on the molecular weight distributions of tars produced under a variety of pyrolysis conditions. The experimental technique has been described in detail elsewhere(Unger and Suuberg,1983a). The widely used heated wire mesh technique was used to pyrolyze small (10-20mg) samples of coal. In these experiments, a thin layer of coal is uniformly spread on a wire mesh which is heated electrically at a predetermined rate to a peak temperature, from which the sample is then immediately recooled without an intervening isothermal period. The mesh is contained inside of a reactor shell which is filled with helium at the desired pressure; the helium remains relatively cold throughout the experiment, as the mesh is the only part of the apparatus which is heated. Since the mesh offers little resistance to escape of volatile products from the thin layer of particles which rest upon it, the volatiles may be assumed to be immediately quenched upon escape from the particle (this point is discussed further below).

Tars are gathered by washing the reactor with tetrahydrofuran (THF) and are analyzed by liquid chromatography for molecular weight distribution. In a few cases, extracts of the chars were obtained by soaking the chars in boiling THF for at least 15 minutes, in an ultrasonic bath. These extracts were analyzed in the same manner as tars for their molecular weights.

In a few cases, tars which had previously escaped the coal particles were reheated in the wire mesh. The sample sizes were roughly 10mg, and the run procedures were identical in every respect to the coal pyrolysis runs.

Finally, a few coal pyrolysis experiments were performed in an atmosphere of pure nitric oxide (NO). Again, the technique was otherwise identical to that used in normal coal pyrolysis experiments.

Table 3 gives elemental compositions of all coals examined in this study.

Results and Discussion

Figure 2 displays molecular weight data for Bruceton standard high volatile bituminous coal tars and extracts. These data will be discussed at length elsewhere (Unger and Suuberg,1983a) and are shown here only as a framework for subsequent discussion. It should be emphasized that the Bruceton coal is a softening coal. Results for non-softening coals will be given below. Several conclusions have been drawn from these data:

-Tars produced at atmospheric pressure are significantly lighter in molecular weight than tars produced at vacuum. The number average molecular weight for the atmospheric pressure tars is typically

between 330 and 350, whereas for vacuum tar it is 430 to 460.

-Both vaouum and atmospheric pressure tars are significantly lighter than the extractable tars left behind in the particle; there is clearly a selective distillation.

-Neither vacuum nor atmospheric pressure tar molecular weight distributions show much sensitivity to temperature.

Subsequent work has revealed several other points(Unger and Suuberg, 1983b):

-There is a low inventory of extractable material present in the particle over the period of most active tar evolution.

-The large difference in yields of atmospheric pressure and vacuum tars develops mainly at peak temperatures in excess of about 550°C. Above this temperature, vacuum tar continues to be evolved, whereas atmospheric tar evolution is virtually complete at this temperature.

The generality of these conclusions is being tested by examining the behavior of a number of other coals. The temperature dependence of the moleoular weight distributions of tars from an Illinois No.6 high volatile bituminous coal, a Pocahontas low volatile ooal and a North Dakota lignite are shown in Figures 3 through 5, respectively. Of these other coals, only the Illinois No. 6 softens during pyrolysis. The behavior of the Illinois No. 6 is very similar to that of the Bruceton coal, including the fact that the molecular weight distribution is relatively independent of temperature. The tar from the North Dakota lignite is likewise very similar in molecular weight range to the tar from the two softening coals. Again, the molecular weight distribution shows little sensitivty to temperature of evolution.

The tar from the Pocahontas coal shows a markedly lower molecular weight range than the tars from the other coals. The number average molecular weight of the Pocahontas tar is 240 at 464°C and 200 at 810°C. As of this writing, no extract molecular weight distribution data are yet available for this coal.

The data which are presently in hand suggest that the evolution of tar during coal pyrolysis is a complex combined transport and reaction process. Clearly, a pure internal liquid phase diffusion limitation cannot explain the trends observed in the softening coals, since it would be impossible to predict a pressure dependence of molecular weight distribution on this basis alone.A simple "batch distillation" transport model is inappropriate, since it would predict increasingly high tar molecular weights with increasing temperature. This has not been observed in any of the coals tested, except over very limited parts of the process (Unger and Suuberg,1983a). The fact that the tars are apparently a light fraction of the extractable molecules present within the particle nevertheless seems to support an evporation controlled mechanism. On this basis, a hypothesis that the evaporation prooess might be essentially analogous to a continuously fed distillation is currently being tested. Other data recently suggested that the pool of evaporating tar is continually being replenished by chemical reactions whose products are basically in a narrow range of molecular weight (Unger and Suuberg,1983b).

As a further test of the hypothesis that evaporation rate controls tar escape from the particle, additional experiments were performed which involved evaporation of pure tars from the wire mesh.

Several milligrams of tar were collected by ordinary methods from the pyrolysis of the Illinois No. 6 coal. This tar was dried and spread in a pure state over the same type of wire mesh as used for coal pyrolysis. Figures 6 and 7 show the results of reheating the tar samples.

Figure 6 shows the molecular weight distribution of the "raw" tar and the molecular weight distributions of the re-evaporated tar fractions. The "raw" tar in Figure 6 differs from the tar products shown in Fig. 3 because drying of any tar sample promotes condensation of light fractions into heavier fractions (as does exposure of tar solutions to light or peroxides). It is apparent from Fig. 6 that tars up to 2000 in molecular weight can indeed evaporate, since no other transport processes were likely to be important in this experiment. It is interesting that upon repyrolysis, the molecular weight distribution of the re-evaporated tar is similar to the original molecular weight distribution of the Illinois No. 6 tar, prior to drying (see Fig. 7).

The above data imply that some degree of true pyrolysis also occurs in the tar re-evaporation experiments. Note in Fig. 6 that there is more light molecular weight material evaporated than was originally present. It is possible that the destruction of high molecular weight species (>2000 in molecular weight) explains why there is relatively much less of this material in re-evaporated tar than in the original coal tar. Alternatively, the presence of such high molecular weight material in the original tar might imply some role of physical entrainment mechanisms during coal pyrolysis, which do not exist in the tar re-evaporation experiments. The physical entrainment picture receives some support from a crude calculation; from the previously presented vapor pressure correlation, the vapor pressure of a 2000 molecular weight species is less than a microtorr at about 450°C. Yet there is a significant amount of such material present in the low temperature tars of all coals studied at that temperature. Of course, there is a great deal of uncertainty in the use of this correlation (derived for considerably lighter, pure hydrocarbons) for coal tars.

Finally, there was some concern that the observed molecular weight distributions might be influenced by secondary gas phase reactions of tar fragments. It was thought that free radical processes were the most likely pathway for such processes, so a crude attempt was undertaken to trap free radicals that might exist in the gas phase. This involved performing the coal pyrolysis experiments in an atmosphere of nitric oxide (NO, a well-known radical trap) rather than helium. It was postulated that if small free radicals were recombining to give larger tar molecules, there would be evidence of a downward shift in the tar molecular weight in NO. The results in Fig. 8 show no such evidence; in fact the average molecular weight of tar species appears to go up in NO. Unfortunately, the test is not clean by any means, since the NO obviously participated in the solid phase chemistry as well.

Conclusions

It now seems apparent that there is a great deal of similarity in the mechanisms of escape of tar from both softening and non-softening coals. The weight of evidence presently appears to favor an evaporation controlled escape of tar from the particle. A simple "batch distillation" model is obviously inappropriate for describing the process. Instead, it seems that a model which allows for simultaneous

tar precursor formation reactions, evaporation processes, and repolymerization reactions is necessary.

References

-Anthony,D.B. and Howard,J.B., AIChEJ, 22,625 (1976).
-Anthony,D.B., Howard,J.B., Hottel,H.C., and Meissner,H.P. 15th Symp. (Int.) on Comb., p1303, 1974.
-Arendt,P. and van Heek,K-H.,Fuel, 60, 779 (1981).
-Attar,A., AIChEJ, 24, 106 (1978).
-Chen,L.W. and Wen,C.Y., ACS Div. of Fuel Chem. Prepr., 24(3), 141 (1979).
-Cheong,P.H., PhD Thesis, California Institute of Technology, Pasadena,Ca. 1977.
-Gavalas,G.R., Coal Pyrolysis, p 104, Elsevier, 1982.
-Gavalas,G.R. and Wilks,K.A., AIChEJ, 26,201 (1980).
-Hiss,T.G. and Cussler,E.L., AIChEJ, 19, 698 (1973).
-Howard,H.C. in Chem. of Coal Util., (H.H. Lowry,Ed.), pp761-773, Wiley, 1945.
-Howard,H.C. in Chem. of Coal Util., Suppl. Vol., (H.H.Lowry, Ed.), pp340-394,Wiley, 1963.
-Howard,J.B. in Chem. of Coal Util., Second Suppl. Vol., (M.A. Elliott,Ed.), pp665-784, Wiley, 1981.
-Howard,J.B., Peters,W.A., and Serio, M.A., EPRI Report AP-1803, Electric Power Research Institute, Palo Alto, Ca., April, 1981.
-James,R.K. and Mills,A.F., Letters in Heat and Mass Transfer, 3, 1 (1976).
-Lewellen, P.C., S.M. Thesis , Dept. of Chem. Eng., M.I.T., Cambridge, Ma. 1975.
-McLean,W.J., Hardesty, D.R., and Pohl, J.H., 18th Symp. (Int.) on Comb., p1239, 1981.
-Melia, P.F. and Bowman,C.T., WSS/CI Paper No. 82-7, Paper presented at the Western States Section/Combustion Institute Meeting, Salt Lake City, Ut., April, 1982.
-Niksa,S., PhD Thesis, Dept. of Chem. Eng., Princeton Univ., Princeton, N.J., 1981.
-Reidelbach,H. and Summerfield,M., ACS Div. of Fuel Chem. Prepr. 20(1), 161 (1975).
-Russel,W.B., Saville,D.A., and Greene,M.I., AIChEJ, 25, 65 (1979).
-Seeker,W.P.,Samuelson,G.S.,Heap, M.P. and Trolinger,J.D., 18th Symp. (Int.) on Comb., p1213, 1981.
-Solomon, P.R. and Colket,M.B., 17th Symp. (Int.) on Comb., p131, 1979.
-Suuberg,E.M., Peters,W.A. and Howard,J.B., I&EC Proc. Des. and Dev., 17, 37 (1978).
---, in Thermal Hydrocarbon Chemistry, (A. Oblad et al., Eds.), ACS Adv. in Chem. Series No. 183, Chap. 14, 1979a.
---, 17th Symp. (Int.) on Comb., p117, 1979b.
-Unger, P.E. and Suuberg, E.M., 18th Symp. (Int.) on Comb., p1203, 1981.
---, Manusoript submitted for publication, 1983a.
---, Manuscript submitted to the International Conference on Coal Science, Pittsburgh,Pa., August, 1983b.
-Zacharias,M.W.,S.M. Thesis, Dept. of Chem. Eng., M.I.T., Cambridge, Ma. 1979.

Acknowledgement

We gratefully acknowledge the support of both the U.S. Department of Energy (Grant DE-FG22-81PC40803) and the Department of Chemical Engineering at CMU. We also thank Marilyn Ley and Glenn Swaney for valuable contributions to this work.

Table 1
Conditions for Figure 1

REFERENCE	SYMBOL	COALS+	PARTICLE SIZE(μ)	HEATING RATE/MAX. TEMP.	PRESSURE (ATM)	METHOD
ARENDT & VAN HEEK (1981)	+	HVB(26), HVB(25), MVB(17), LVB(9)	200-315	200°C/s 1000°C	0.1-90	HWM
GAVALAS & WILKS (1980)	✪	HVB(19), SUBB(6)	110	600°C/s 500°C	0.1-2	HWM
SUUBERG ET AL.(1978,1979)	●	LIGNITE(8) HVB(36)	53-88	1000°C/s >900°C	10^{-4}-69	HWM
UNGER & SUUBERG(1983b)	⊞	HVB(36)	62-88	1000°C/s >900°C	10^{-4}-1	HWM
H.C.HOWARD (1945)	△	HVB(20)	400-800	1°C/s 525°C	10^{-4}-1	RETORT
*ANTHONY ET AL. (1974)	■	HVB	70	>650°C/s 1000°C	10^{-3}-69	HWM
*NIKSA (1981)	×	HVB	125	1000°C/s 750°C	10^{-4}-100	HWM

* Tar yield data estimated
\+ Maximum observed tar yields under vacuum shown in paretheses
HWM= Heated Wire Mesh

Table 2
Comparison of Predicted and Measured Temperatures
for a Vapor Pressure of 0.5mmHg (°C)

Compound	MW	Meas. Temp.	Calc. Temp.
1-t-Butyldecahydro-naphthalene	198	59.5	71.2
1,2-Diphenylbenzene	231	124.0	115.3
Perhydroperylene	262	150.5	145.1
3-n hexylperylene	336	198.0	210.8
2-n octylchrysene	339	242.5	213.3
3-n decylpyrene	342	235.5	215.8

MW=Molecular Weight
Vapor pressure data from G.Smith,J.Winnick,D.Abrams, and J. Prausnitz, Can. J. Chem. Eng.,54,337(1976).

Table 3
Ultimate Analyses of Coals Examined

COAL	C	H	O	N	S	ASH	MOISTURE
BRUCETON PITTS. NO.8 BITUMINOUS	80.4	5.3	6.7	1.6	1.0	4.6	1.7
HILLSBORO ILL. NO. 6 BITUMINOUS	67.2	4.6	12.3	1.2	3.4	11.7	8.6
W.VA. POCAHONTAS LOW VOLATILE BITUM.	84.4	4.2	3.7	0.3	0.5	6.8	0.2
NORTH DAKOTA LIGNITE	66.7	3.7	19.5	0.9	0.8	9.3	32.4

All results on a dry basis except moisture, which is reported on an as-received basis. North Dakota lignite is dried prior to use.

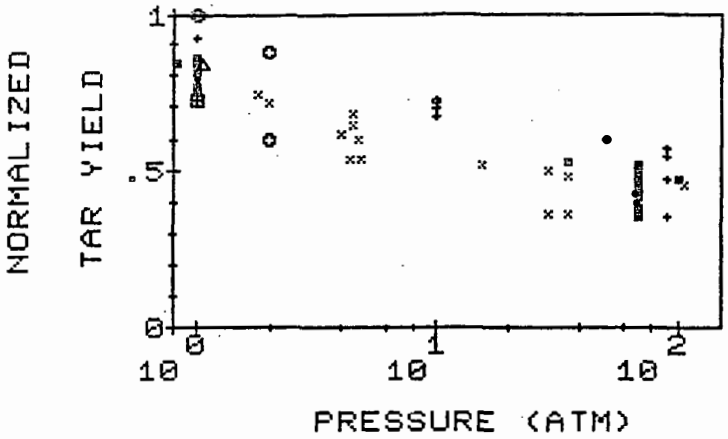

FIGURE 1. VARIATION OF TAR YIELD WITH PRESSURE OF INERT GAS EXTERNAL TO THE PARTICLE DURING PYROLYSIS. SEE TABLE 1 FOR EXPLANATION OF SYMBOLS.

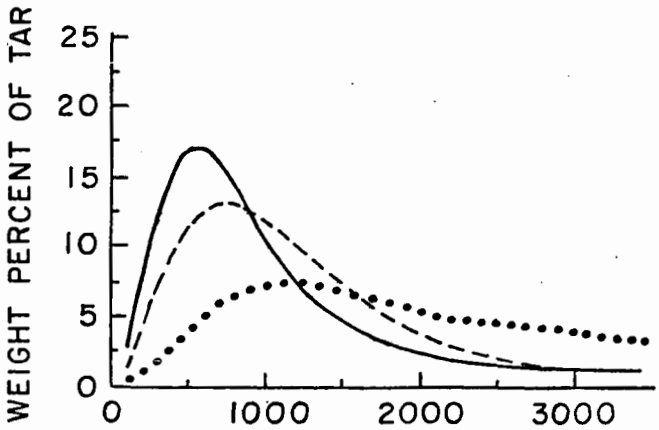

FIGURE 2. MOLECULAR WEIGHT DISTRIBUTIONS OF BRUCETON COAL TARS AND EXTRACTS. SOLID CURVE-ATMOSPHERIC PRESSURE TAR; DASHED CURVE-VACUUM TAR; DOTTED CURVE-COAL EXTRACT. ALL FOR SAMPLES HEATED AT 1000°C/s TO 546°C, FOLLOWED BY COOLING AT 200-400°C/s.

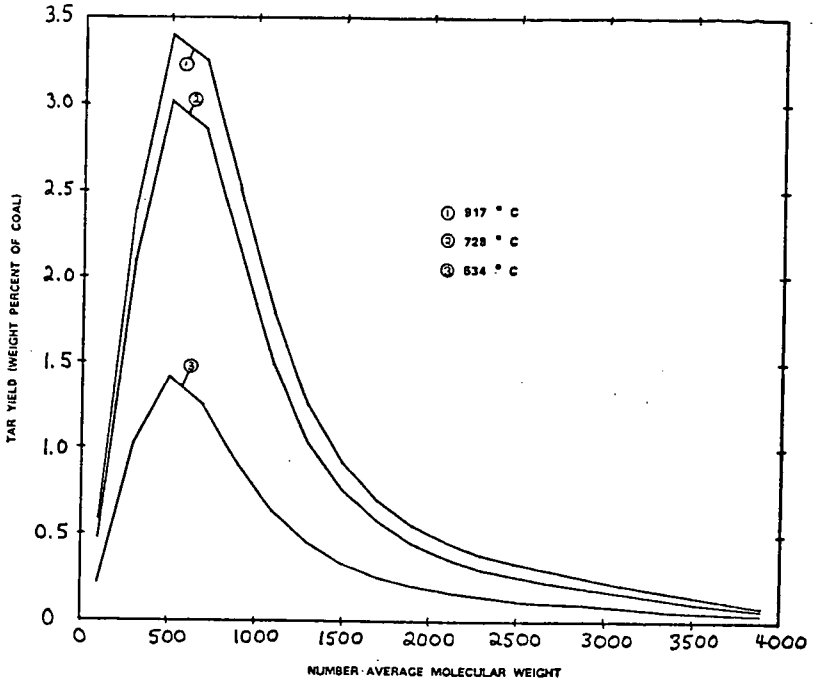

FIGURE 3. MOLECULAR WEIGHT DISTRIBUTIONS OF ILLINOIS NO. 6 ATMOSPHERIC PRESSURE TAR. SAMPLES HEATED AT 1000°C/s TO INDICATED TEMPERATURES.

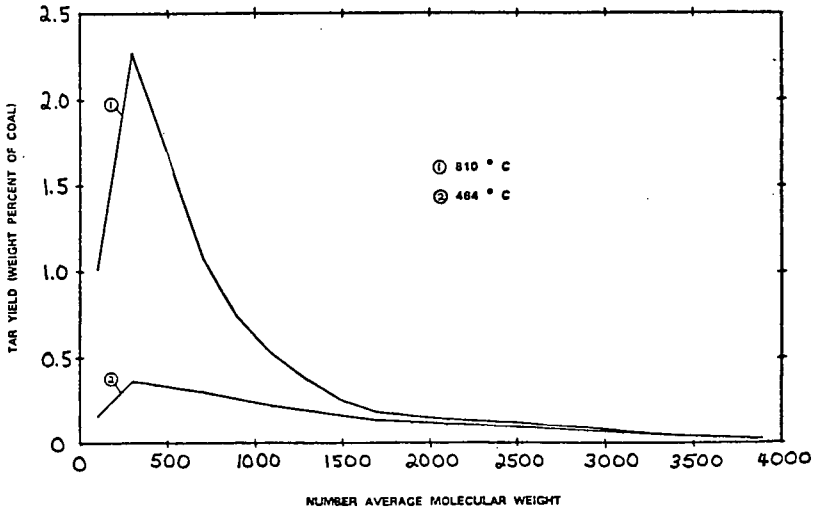

FIGURE 4. MOLECULAR WEIGHT DISTRIBUTIONS OF POCAHONTAS LOW VOLATILE COAL ATMOSPHERIC PRESSURE TAR. SAMPLES HEATED AT 1000°C/s TO INDICATED TEMPERATURES.

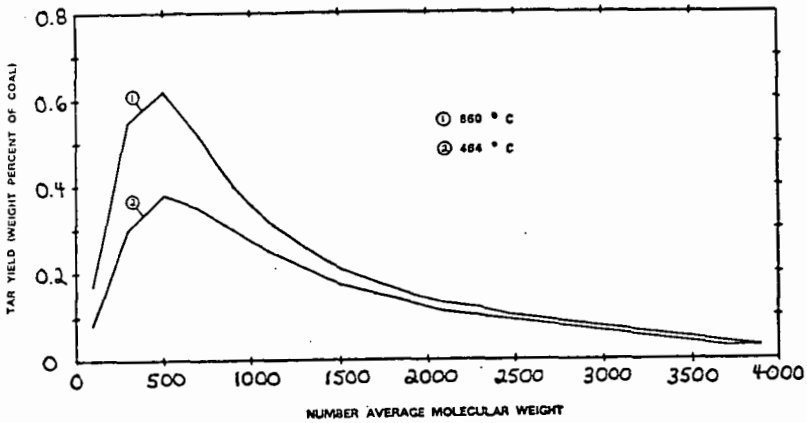

FIGURE 5. MOLECULAR WEIGHT DISTRIBUTIONS OF NORTH DAKOTA LIGNITE ATMOSPHERIC PRESSURE TAR. SAMPLES HEATED AT 1000°/S TO INDICATED TEMPERATURES.

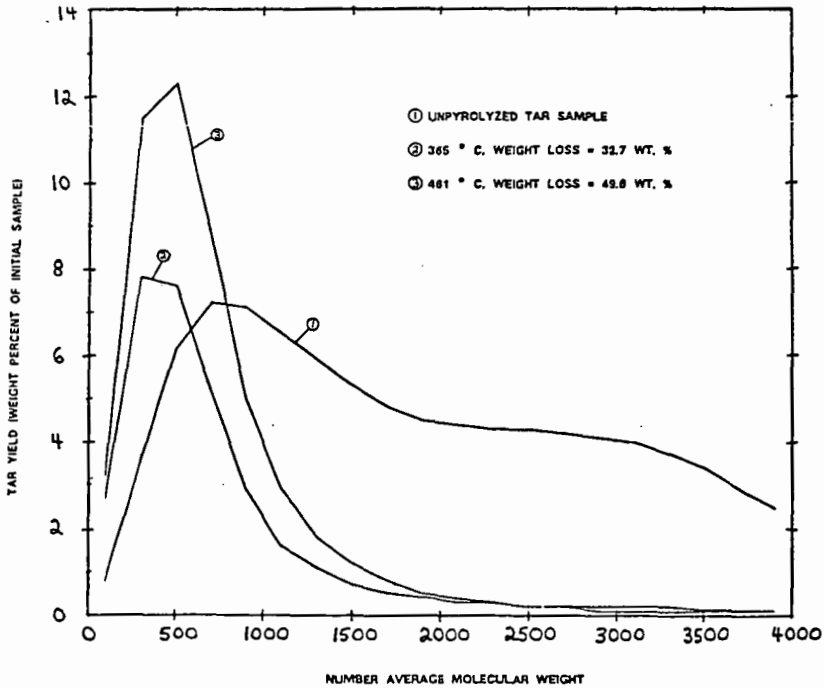

FIGURE 6. MOLECULAR WEIGHT DISTRIBUTIONS OF DRIED "RAW" ILLINOIS NO. 6 TAR, AND RE-PYROLYZED (RE-EVAPORATED) FRACTIONS OF THAT TAR. SAMPLES HEATED AT 1000°C/S TO THE INDICATED TEMPERATURES.

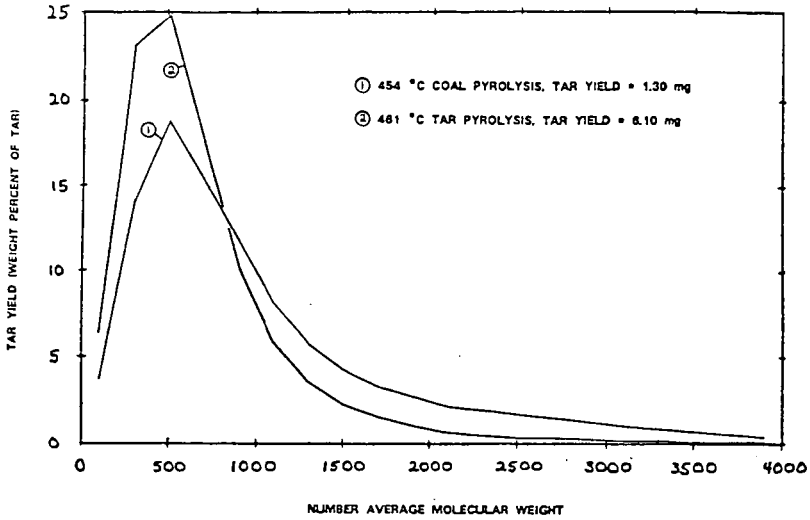

FIGURE 7. A COMPARISON OF THE MOLECULAR WEIGHT DISTRIBUTIONS OF FRESH ILLINOIS NO. 6 TAR (FROM COAL PYROLYSIS) AND RE-PYROLYZED TAR. THESE SAMPLES WERE FORMED UNDER NEARLY IDENTICAL HEATING CONDITIONS (1000°C/S HEATING RATES).

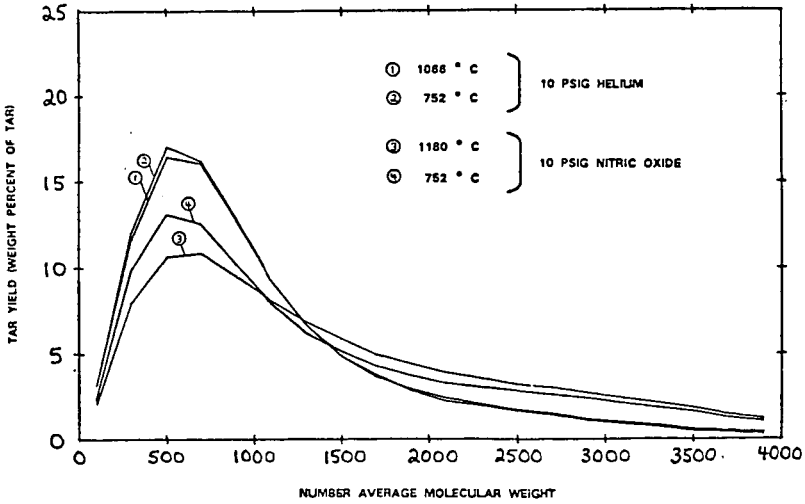

FIGURE 8. A COMPARISON OF MOLECULAR WEIGHT DISTRIBUTIONS OF TARS PRODUCED BY PYROLYSIS OF BRUCETON COAL UNDER HELIUM AND NITRIC OXIDE.